Interpreting Summertime Hourly Variation of NO_2 Columns with Implications for Geostationary Satellite Applications

Deepangsu Chatterjee[1], Randall V. Martin[1], Chi Li[1], Dandan Zhang[1], Haihui Zhu[1], Daven K. Henze[2], James H. Crawford[3], Ronald C. Cohen[4,5], Lok N. Lamsal[6], Alexander M. Cede[6]

[1]Department of Energy, Environmental & Chemical Engineering, Washington University in St. Louis, St. Louis, MO, USA
[2]Department of Mechanical Engineering, University of Colorado, Boulder, CO, USA
[3]NASA Langley Research Center, Hampton, VA, USA
[4]Department of Chemistry, University of California, Berkeley, Berkeley, CA, USA
[5]Department of Earth and Planetary Science, University of California, Berkeley, Berkeley, CA, USA
[6]NASA Goddard Space Flight Center, Greenbelt, MD 20771, USA

Correspondence: Deepangsu Chatterjee (deepangsuchatterjee@wustl.edu)

Abstract

Accurate representation of the hourly variation in the NO_2 column-to-surface relationship is essential for interpreting geostationary observations of NO_2 columns. Previous research indicated inconsistencies in this hourly variation. This study employs the high-performance configuration of the GEOS-Chem model (GCHP) to analyze daytime hourly NO_2 total columns and surface concentrations during summer. We use measurements from globally distributed Pandora sun photometers and aircraft observations over the United States. We correct Pandora total NO_2 vertical columns for 1) hourly variations in effective temperature driven by vertically-resolved contributions to the total column and 2) changes in local solar time along the Pandora line-of-sight. These corrections increase the total NO_2 columns by 5-6 × 10^14 molecules cm^{-2} at 9 AM and 6 PM across all sites. Fine scale simulations from GHCP (~12 km) reduce the Normalized Bias (NB) against Pandora total NO_2 columns from 19% to 10% and against aircraft measurements from 25% to 13% in Maryland, Texas, and Colorado. Similar reductions are observed in NO_2 columns over eastern US (17% to 9%), western US (22% to 14%), Europe (24% to 15%), and Asia (29% to 21%) when compared to 55 km simulations. Our analysis attributes the weaker hourly variability in the total NO_2 column to 1) hourly variations in column effective temperature, 2) local solar time changes along the Pandora line-of-sight, and 3) differences in hourly NO_2 variability from different atmospheric layers, with the lowest 500 m exhibiting greater variability, while the dominant residual column above 500 m exhibits weaker variability.

1 Introduction

Nitrogen oxides ($NO_x \equiv NO + NO_2$) affect air quality and human health directly by contributing to premature mortality (Burnett et al., 2004; Tao et al., 2012) and asthma for children and adults (Anenberg et al., 2018), and indirectly by acting as precursors for tropospheric ozone (O_3) formation (Jacob et al., 1996), and nitrate aerosols (Bauer et al., 2007). Significant spatial gaps in ground-based monitoring of surface NO_2 concentrations and pronounced NO_2 heterogeneity inhibit exposure assessment. To fill in the knowledge of NO_2 exposures across a greater fraction of the human population, satellite remote sensing offers the potential for spatially comprehensive measurements. Major advances in satellite remote sensing from sun-synchronous low earth orbit (LEO) has achieved global characterization of tropospheric NO_2 columns at specific times of the day (Duncan et al., 2013; Veefkind et al., 2012) that have been applied to infer ground level NO_2 concentrations (Anenberg et al., 2022; Lamsal et al., 2011; Geddes and Martin, 2017; Cooper et al., 2022). The emerging geostationary constellation (Al-Saadi et al., 2017) including the Geostationary Environmental Monitoring Spectrophotometer (GEMS) over Asia, Tropospheric Emissions: Monitoring Pollution (TEMPO) over North America, and Sentinel-4 over Europe offers the prospect of inferring spatially comprehensive maps of hourly ground-level NO_2 concentrations. Toward this goal, there is a need to develop an accurate representation of the hourly NO_2 column to surface relationship.

Understanding the hourly variation of the relationship of NO_2 columns with surface concentrations is of particular interest due to its role in the inference of hourly surface NO_2 from satellite remote sensing. Numerous studies have separately examined the role of processes such as surface emissions, boundary layer mixing, chemistry, deposition, and advection (Yang et al., 2023b; Herman et al., 2009; Ghude et al., 2020; Zhang et al., 2016) upon the hourly variation of NO_2 columns and upon surface NO_2 concentrations in the United States (Day et al., 2009), Spain

(Van Stratum et al., 2012), India (David and Nair, 2011), South Korea (Yang et al., 2023a, b) and China (Tong et al., 2017). Differences have been identified in the daytime hourly variation of NO_2 tropospheric columns and surface concentrations during the DISCOVER-AQ and KORUS-AQ (Korea US -Air Quality) campaigns with pronounced variation in surface concentrations that is not evident in the columns (Choi et al., 2020; Crawford et al., 2021). Differences have also been noted in hourly variation of NO_2 measured by aircraft and ground-based Pandora instruments (Li et al., 2021). There is a need to understand the factors that can affect the relationship of hourly NO_2 columns with surface concentrations.

Major challenges in the interpretation of satellite NO_2 observations include the short lifetime of NO_x (Laughner and Cohen, 2019), and localized emissions (Crippa et al., 2018) that affect its spatial heterogeneity. Course resolution inputs to satellite retrieval algorithms (e.g., terrain height, albedo, and a priori NO_2 profiles) can lead to biases (Laughner et al., 2019; Laughner et al., 2018; Russell et al., 2011). Complications with ground-based measurements of the NO_2 columns as part of Pandora include uncertainties at steeper solar zenith angles during morning and evening hours (Herman et al., 2009; Reed et al., 2015) and the changing Pandora field of view (FOV) during morning and late evening (Li et al., 2021). Non-linearities in the relationship between NO_2 concentrations and NO_x sources or sinks can lead to biases in coarse-resolution chemical transport models (CTMs) (Valin et al., 2011) that necessitate CTMs with a finer resolution (Li et al., 2021, 2023a). Recent advances in the simulation of global atmospheric composition at fine resolution (Eastham et al., 2018; Hu et al., 2018; Martin et al., 2022) offer the opportunity to address the resolution need at the global scales of the geostationary constellation.

An important consideration in the inference of surface NO_2 concentrations with columnar satellite observations is the vertical profile of NO_2 concentrations. Aircraft observations from the

NASA Deriving Information on Surface Conditions from Column and Vertically Resolved Observations Relevant to Air Quality (DISCOVER-AQ) campaign offers measurements of the NO_2 vertical profile in the lower troposphere for evaluation of modeled vertical profiles (Flynn et al., 2014; Reed et al., 2015). The Pandonia Global Network (PGN) is a global sun photometer network that offers hourly measurements of total NO_2 columns (Verhoelst et al., 2021), useful for interpretation of the daytime variation of NO_2 columns and evaluation of simulated columns. In this study, we interpret the summertime NO_2 measurements from the NASA P-3B aircraft using the high-performance GEOS-Chem (GCHP) simulations along aircraft flight tracks and account for line-of-sight of the Pandora sun photometers over Maryland, Texas, and Colorado during the DISCOVER-AQ campaign. We also explore the effect of vertical changes in the hourly variation of temperature on the NO_2 cross-section and the raw Pandora columns. We further investigate the hourly variation of NO_2 columns and surface concentrations from 50 PGN sites across the northern hemisphere. Section 2 describes the datasets and methods used in this study to interpret the variation of NO_2 columns, surface concentrations, and vertical distribution over DISCOVER-AQ and PGN sites. Section 3 examines the consistency between the NO_2 vertical columns and surface concentrations across DISCOVER-AQ sites, and PGN sites across the contiguous United States (CONUS), Europe, and Asia. We explore the effects of model resolution and boundary layer height adjustments on the hourly variation of NO_2 total columns and surface concentrations as a function of hourly variation in mixed layer depth and photochemistry, and measurement characteristics of Pandora sun photometers over PGN sites across the CONUS, Europe, and Asia.

2 Materials and Methods

2.1 Aircraft measurements of NO_2 vertical profiles

The DISCOVER-AQ campaign offers comprehensive datasets of airborne and surface observations relevant for accessing air quality. One of the main objectives of the campaign was to examine the hourly variation of the relationship between the column and surface concentrations. In this study, we use aircraft, Pandora, and surface measurements over Maryland (July 2011), Texas (September 2013) and Colorado (July-August 2014) to investigate the hourly variation of NO_2 vertical profiles during summer when a long duration of daylight exists for analysis. Figure A1 shows the flight tracks, altitude variation, roadways, and Pandora instrument locations over Maryland, Texas, and Colorado during the DISCOVER-AQ campaign. We focus on the aircraft spirals since they are designed to sample the vertical profile. We use NO_2 concentrations measured by the thermal dissociation laser-induced fluorescence (TD-LIF) technique (Thornton et al., 2000; Day et al., 2002) during the campaign. The laser-induced fluorescence method is highly sensitive for directly measuring NO_2, with a measurement uncertainty of 5 % and a detection limit of 30 pptv (Thornton et al., 2000). It also attempts to correct for positive interferences (Nault et al., 2015; Yang et al., 2023b). We use aircraft measurements from a height of about 300 m above ground level (AGL) up to 4 km AGL where high measurement frequency facilitates regional representation.

2.2 Pandonia Global Network NO_2 Total Column Densities

PGN is a global network of ground-based sun photometers that measure sun and sky radiance from 270 to 530 nm that allow retrievals of various trace gases including NO_2. Retrieval precision for total vertical NO_2 columns ("NO_2 columns" hereafter) is 5.4×10^{14} molecules/cm^2 with a nominal accuracy of 2.7 x 10^{15} molecules/cm^2 under clear-sky conditions (Herman et al., 2009; Cede 2021). We obtained the level 2 data product from the version rnvs3p1-8 for PGN and DISCOVER-AQ (data source listed in the code and data availability section). We also include surface NO_2 observations from co-located DISCOVER-AQ and PGN sites. We use NO_2 columns and surface concentrations employed during the DISCOVER-AQ campaign from 18 sites over Maryland, Texas and Colorado. We also include NO_2 columns and surface concentrations from 50 PGN sites (the US: 31, Europe: 10, Asia: 9) for June-July-August (JJA) 2019. We focus on the NO_2 observations between 9 AM - 6 PM local solar time, for consistency in observation frequency across all PGN sites. Tables A1 and A2 contain the names and locations of the DISCOVER-AQ and PGN sites respectively. We exclude Pandora measurements with SZA>80°. We use total NO_2 columns including the stratosphere because the use of external information sources to remove the stratospheric NO_2 columns from PGN can introduce errors in the residual tropospheric columns (Choi et al., 2020).

2.3 GEOS-Chem simulations

We use GCHP, the high-performance configuration of the GEOS-Chem model that operates with a distributed-memory framework for massive parallelization (Eastham et al., 2018), to interpret the NO_2 column, vertical distribution and surface observations. GCHP offers the ability to simulate the entire atmospheric column needed to interpret Pandora measurements and the fine spatial resolution needed to interpret aircraft measurements. GEOS-Chem is driven by assimilated meteorological data from the NASA Goddard Earth Observation System (GEOS). GEOS-Chem includes a comprehensive O_x-NO_x-VOC-halogen-aerosol chemical mechanism in the troposphere, in addition to the unified tropospheric-stratospheric chemistry extension in the stratosphere (Eastham et al., 2014). We use GEOS-Chem 14.1.1 which includes recent updates to GCHP (Martin et al., 2022), NO_x heterogenous and cloud chemistry (Holmes et al., 2019), isoprene chemistry (Bates and Jacob, 2019), and aromatic chemistry (Bates et al., 2021). The ISORROPIA II module simulates the thermodynamic partitioning between the gas and condensed phase (Fountoukis and Nenes, 2007). Natural emissions include biogenic volatile organic compounds

(VOCs) (Weng et al., 2020), lightning NO_x (Murray et al., 2012), and soil NO_x (Weng et al., 2020). GEOS-Chem includes an updated aircraft NOx emissions inventory for 2019, developed with the Aircraft Emissions Inventory Code (Simone et al., 2013). Figure A2 shows the hourly variation of NO_x emissions across the PGN sites. For the interpretation of PGN measurements in 2019, we conduct the simulations for the year 2019 using GEOS-FP meteorology and the stretched grid capability (Bindle et al., 2021) at a cubed sphere resolution of C180 (~55 km) and stretch factor of 4.0 yielding a regional refinement of ~12 km. All simulations were conducted with a two-week spin-up. We interpolate hourly GCHP outputs of simulated NO_2 columns and surface concentrations to the local solar time at the PGN observation sites.

For interpretation of the DISCOVER-AQ aircraft campaigns, we conduct stretched grid simulations over Maryland (July 2011), Texas (September 2013) and Colorado (July-August 2014) with identical stretched grid configurations, with sampling along the aircraft flight tracks. We use MERRA-2 meteorology for these simulations as GEOS-FP meteorology datasets are not available prior to 2014. A sensitivity test for the year 2019 using either GEOS-FP and MERRA-2 affects the local simulated NO_2 columns and surface concentrations by less than 5% for both 12 km and 55 km resolutions.

Hourly variation of the planetary boundary layer height (PBLH) can influence the vertical distribution and hence the surface concentration of aerosols and trace gases (Lin and McElroy, 2010). Millet et al., (2015) found that GEOS-FP reanalysis over-estimates daytime PBLH as compared to observations; correcting for PBLH estimations can lead to a better agreement of ozone (Oak et al., 2019) and $PM_{2.5}$ (Li et al., 2023b) with measurements. Our base case simulation uses the PBLH derived from the Aircraft Meteorological Data Reports (AMDAR) at 54 sites across the CONUS to adjust the PBLH estimates as described in Li et al., (2023). We examine the effect of using the adjusted PBLH for simulations over the CONUS, Europe and East Asia. Table 1 shows the 3 simulation cases conducted over Maryland, Texas, Colorado, the CONUS, Europe and East Asia.

Table 1. Summary of GCHP Simulations

Name	Description
Base_12	12 km base
NoΔBL_12	12 km without PBLH modification
NoΔBL_55	55 km without PBLH modification

2.5 Effective temperature of Pandora measurements

The NO_2 cross section is temperature dependent with the magnitude of spectral features in a 294 K NO_2 spectrum about 80% of those in 220 K NO_2 spectrum (Vandaele et al., 2002). Thus, the NO_2 columns fitted with a 220 K NO_2 spectrum are about 80% of those fitted with the 294 K NO_2 spectrum. Prior studies have identified biases in the Pandora total ozone column effective temperature driven by variations in seasonal temperature (Zhao et al., 2016; Herman et al., 2015). To account for the hourly variations in temperature vertical profiles, we calculate simulated NO_2 effective temperatures T_{eff} using the site-specific hourly GEOS-FP temperature profiles $(T)_i$, NO_2 cross section $\sigma(NO_2)_i$, and GCHP NO_2 vertical profiles $VC(NO_2)_i$ following equation (1) of Herman et al. (2009):

$$T_{eff} = \frac{\sum_i^N(\sigma(NO_2)_i \,.\, VC(NO_2)_i \,.(T)_i\,))}{\sum_i^N(\sigma(NO_2)_i \,.\, VC(NO_2)_i\,))} \qquad (1)$$

The comparison between GCHP simulated and Pandora observed effective temperature is discussed in sec 3.2.

2.6 Local solar time along Pandora line-of-sight

At observing scenarios with large solar zenith angles, the Pandora sun photometer observes air masses with varying local solar time at different altitudes along the line-of-sight. This feature is particularly noteworthy for comparing hourly Pandora observations with other measurements or simulations. Figure 1 shows the sampling process of GCHP simulations along the line-of-sight of the Pandora sun photometer. GCHP grid boxes are integrated along the viewing geometry of the Pandora instrument to create a “staircase column” that accounts for the effects of local solar time on the horizontal and vertical variation in NO_2 concentrations. The variation in local solar time is most relevant near sunrise and sunset when the NO_2/NOx ratios change rapidly as discussed in section 3.2. We correct the vertical columns reported by PGN to the local solar time of the instrument by applying the ratio of integrated staircase columns to vertical columns.

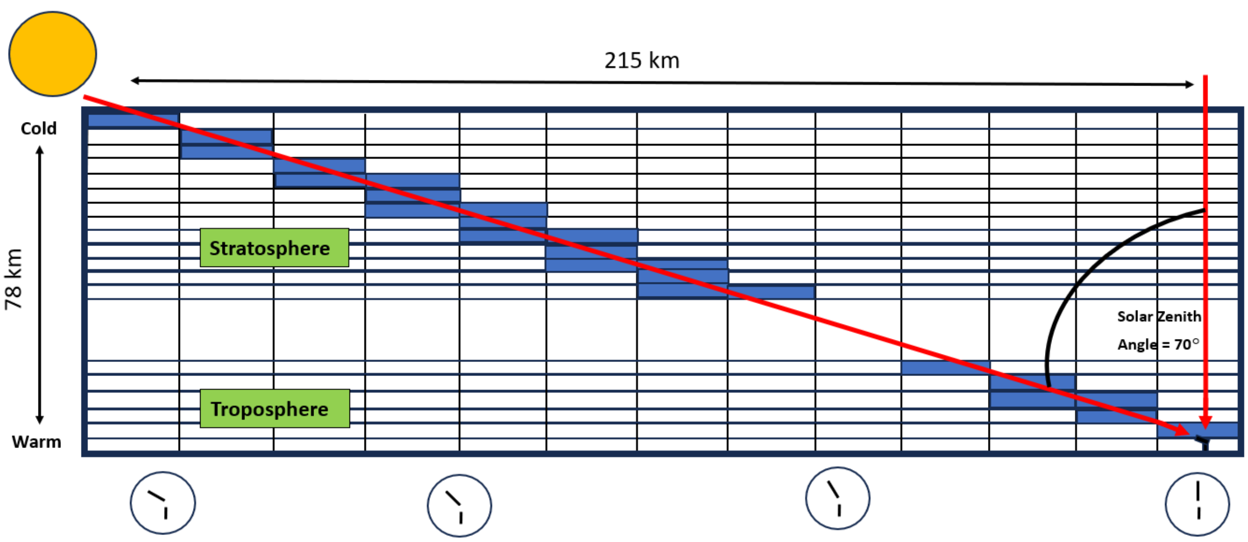

Figure 1. Configuration of integrating the GCHP grid boxes along the line-of-sight of the Pandora instrument. The shaded grid boxes represent the line-of-sight for the Pandora sun photometer at an inclined solar zenith angle. Clock faces indicate a change in local solar time.

2.7 Ground based surface NO_2 measurements

We use hourly NO_2 surface concentrations from the catalytic converter measurements over

DISCOVER-AQ and PGN sites. Based on the approach of Lamsal et al., (2008) and Shah et al., (2020), we correct the interference of organic nitrates and HNO_3 in the NO_2 measurements, using a correction factor derived from GCHP simulated site-specific NO_2, organic nitrates, and HNO_3 mixing ratios. The correction for HNO_3 and organic nitrates reduced the summertime mean NO_2 surface concentrations by 18% over DISCOVER-AQ sites and 23% over PGN sites.

2.8 Normalized Bias

We use normalized absolute bias or normalized bias (NB) to evaluate the simulations. The NB is calculated using the following equation-

$$NB = \frac{\sum_{i=1}^{N} |S_i - O_i|}{\sum_{i=1}^{N} O_i} \times 100\% \quad (2)$$

where, O_i is the observation and S_i is the corresponding simulated value, i refers to the index of the observation and N refers to the total number of observations.

3 Results and Discussion

3.1 Hourly variation of observed and simulated NO_2 vertical profiles

Figure 2 shows the hourly variation in the airborne TD-LIF measurements and simulated NO_2 vertical profiles at 12 km resolution (Base_12) over Maryland, Texas and Colorado during the DISCOVER-AQ campaign. The measurements exhibit a pronounced maximum at 500 m at 10 AM (squares) that diminishes by a factor of 2 in the afternoon as concentrations become more uniform below 1.5 km (triangles and diamonds), driven by the hourly variation in PBLH mixing from early morning to late afternoon. For all three DISCOVER-AQ campaigns, the 12 km simulated NO_2 mixing ratios represent the vertical profile well with normalized bias (NB) below 16% at local times: 10 AM, 2 PM, and 5 PM. Differences tend to be larger within 1-2 km above ground level in the afternoon (2 PM and 5 PM local time), which integrates to a lower simulated partial column of 6 x 10^{14} molecules cm^{-2}. The simulated NO_2 vertical profiles at 12 km without PBLH modifications (NoΔBL_12) are similar to those with the PBLH modification (Figure A3). Figure A4 shows the 55 km simulated NO_2 vertical profiles (NoΔBL_55). The 55 km GCHP simulations have increased NB by a factor of 2, as compared to 12 km. Overall, the NO_2 vertical profile exhibits greater consistency with observations at 12 km than at 55 km by better resolving

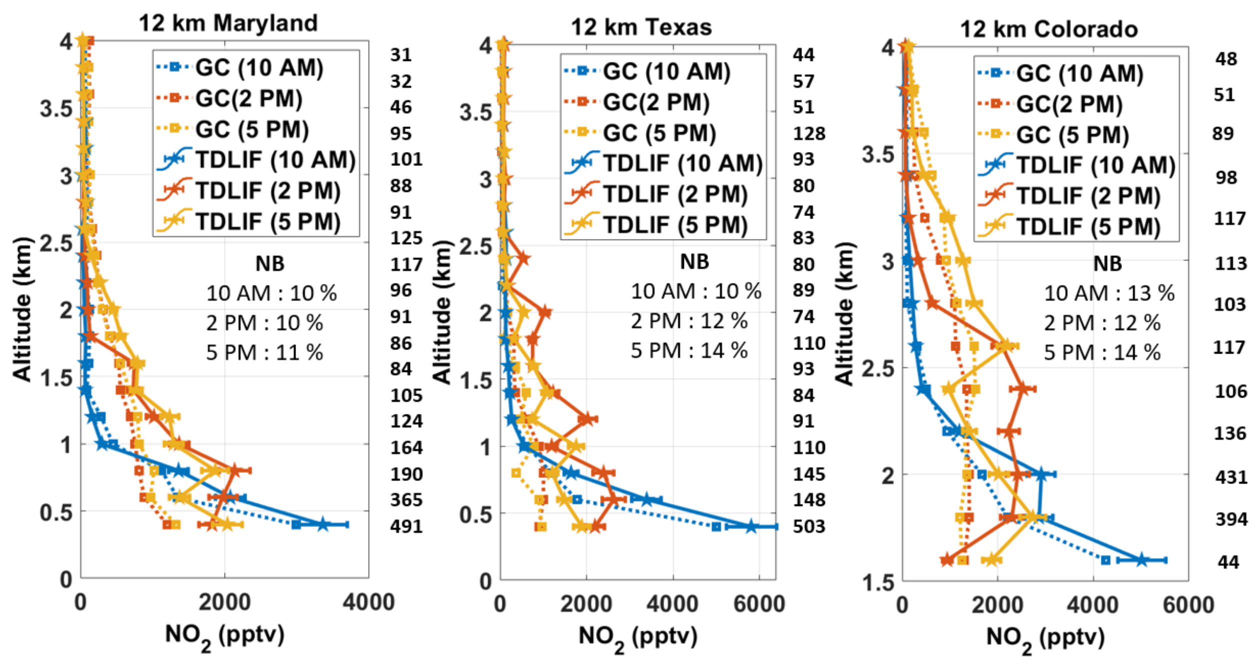

Figure 2: NO_2 vertical profiles from TD-LIF instrument aboard P-3B during the DISCOVER-AQ campaign over Maryland, Texas, and Colorado. The colored solid lines with pentagram markers represent observations. The dotted colored lines with square markers represent 12 km GCHP simulated mixing ratios. The inset values in the boxes show the normalized biases (NBs) at 10 AM, 2 PM, and 5 PM. The numbers on the right of each panel represent the number the observations associated with the corresponding altitude level. Error bars indicate standard errors in measurements.

the heterogeneous conditions along the aircraft flight tracks.

3.2 Corrections to Pandora Effective Temperature

The left panel in Figure 3 shows the Pandora and simulated mean hourly effective temperature of the NO_2 columns over all PGN sites during June-August as inferred using hourly GEOS-FP temperature profiles and GCHP NO_2 vertical profiles. The Pandora effective temperatures exhibit weak hourly variation with a warmer temperature at the Asian sites where boundary layer NO_2 concentrations are typically higher than in the US and Europe. The GCHP simulated effective temperature is also warmer for Asian sites, however, the effective temperature is lower during the early afternoon when near-surface NO_2 concentrations tend to be minimum such that the stratospheric NO_2 makes a larger fractional contribution to the total column. The simulated effective temperature further deviates from the Pandora effective temperature with an increase toward sunrise and sunset with contributing to higher surface NO_2 concentrations. The corresponding correction factor (CF) for hourly variation in the effective temperature is calculated as:

$$\mathrm{CF} = 1 + \left(\frac{1}{0.8} - 1\right) \times \frac{\left(T_{eff}\left(GCHP(hour)\right) - T_{eff}\left(Pandora(hour)\right)\right)}{294-220} \quad (3)$$

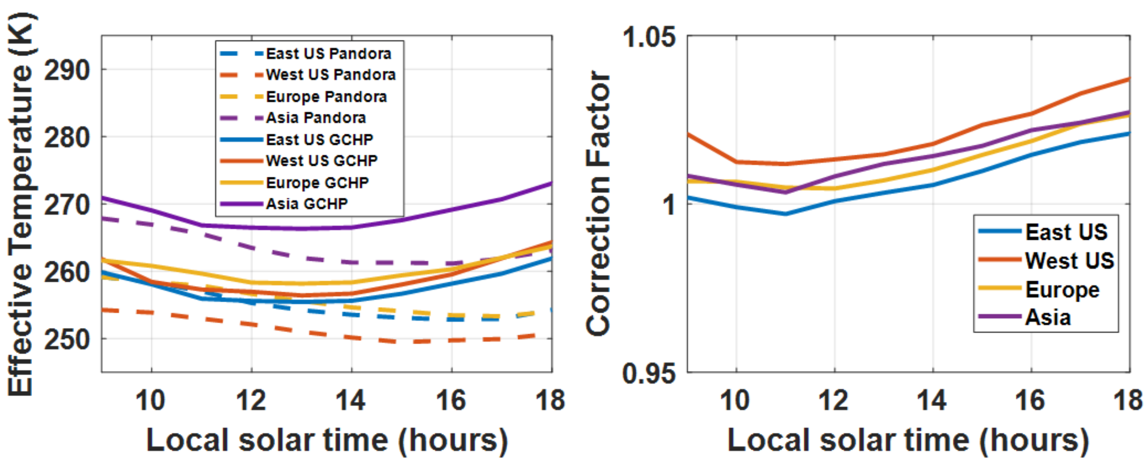

Figure 3. Hourly variation of the total NO_2 column mean effective temperature across all PGN sites (left panel) and the corresponding correction factors (right panel).

The factor of $\left(\frac{1}{0.8} - 1\right)$ reflects the difference between the NO_2 columns fitted with a 220 K NO_2 spectrum that are about 80% of those fitted with a 294 K NO_2 spectrum. The CF for the Pandora NO_2 columns increases toward sunrise and sunset due to the increased effective temperature, reflecting the greater abundance of NO_2 molecules observed per unit absorption. We apply site-specific CFs across all Pandora observations.

3.3 Hourly variation of observed and simulated NO_2 VCDs

Figure 4 (left) shows the mean hourly daytime Pandora vertical NO_2 columns summarized from the summertime DISCOVER-AQ campaign measurements. The raw Pandora NO_2 columns exhibit weak hourly variation of 8×10^{14} molecules cm^{-2} (within 10% of the daytime mean) that is inconsistent with the aircraft measurements that indicate total columns in the morning and

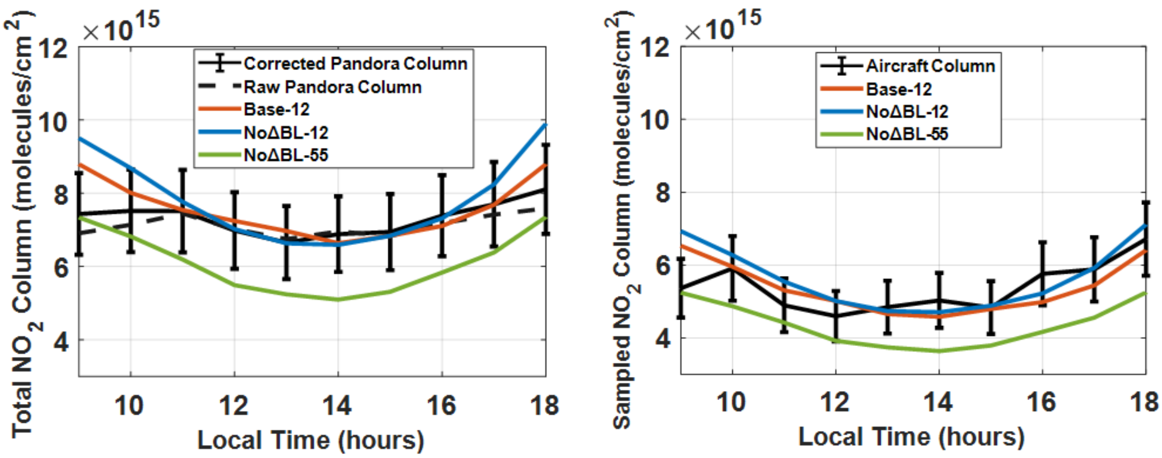

Figure 4. The left panel shows the total NO_2 vertical columns from corrected DISCOVER-AQ Pandora columns (black), raw DISCOVER-AQ Pandora columns (black dotted), the 12 km base case simulation (red), 12 km without modified PBLH (blue) and 55 km without modified PBLH (green), during the DISCOVER-AQ campaigns over Maryland (2011), Texas (2013) and Colorado (2014). The corrected Pandora columns account for the hourly variation in the effective temperature and the local solar time along the line-of-sight. The right panel shows sampled aircraft and simulated partial columns (300 m A.G.L - 4 km A.G.L). Error bars indicate standard error.

evening of about 1.5×10^{15} molecules cm^{-2} greater than afternoon. The corrected Pandora measurements that account for hourly variation in effective temperature and local solar time along line-of-sight exhibit greater NO_2 columns in morning and evening by about 1.3×10^{15} molecules cm^{-2}, similar to the aircraft measurements. Since the Pandora instruments track the sun, viewing stratospheric air masses 100 - 200 km away from the measurement station to the East in the morning and to the West in the evening, the local solar time of stratospheric NO_2 observed by

Pandora instruments near sunrise and sunset is systematically shifted by about 5-10 mins towards noon. This shift can be particularly important during sunrise and sunset when NO_2 columns in the stratosphere undergo a pronounced increase driven by an increasing NO_2/NOx ratio (Figure A5). The 12 km simulated vertical columns generally represent the corrected Pandora observed columns with an NB of 10%. Excluding the PBLH modification would have increased the NB to 13%. Using a coarser 55 km simulation would have further degraded the agreement with an NB of 19%. We sample the GCHP simulated NO_2 columns between 300 m and 4 km to compare with the aircraft columns (right panel). The hourly variation of partial NO_2 columns over 300 m to 4 km AGL from aircraft observations exhibits a distinct increase in morning and evening and are well represented by the 12 km base case simulation (NB = 13%). Similar to our analysis for Pandora sites, excluding the PBLH modification and coarsening the simulation to 55 km degrades the performance (NB = 15% and 25%) versus aircraft columns.

Figure 5 extends our analysis to all PGN sites across the CONUS, Europe and East Asia. Raw measurements across all regions exhibit weak hourly variation. The correction for effective temperature and local solar time along the Pandora line-of-site increases the mean NO_2 columns in the morning and evening by about 6×10^{14} molecules cm^{-2} across all regions. The base case simulation generally reproduces measurements with NB of 9% for the eastern US, 14% for the western US, 15% for Europe and 21% for east Asia sites. Excluding the PBLH correction would have increased the NB (eastern US: 12%, western US: 18%, Europe: 18%, and eastern Asia: 26%) with the largest change in Asia. Excluding the PBLH correction yields a higher daytime PBLH resulting in increased chemical lifetime of NO_x, reduced NO_2 dry deposition rates and increased NO_2/NO_x ratio during afternoon and evening (Figure A6), thus leading to an hourly variation that deviates from the Pandora observations. Coarser resolution generally further increases the bias, reflecting resolution effects discussed in the next section. The increase of the simulated total NO_2 columns between 3-6 PM across all PGN sites reflects an increase in the NO_2/NO_x ratio throughout the column, driven by a reduction in HO_x (Figure A7).

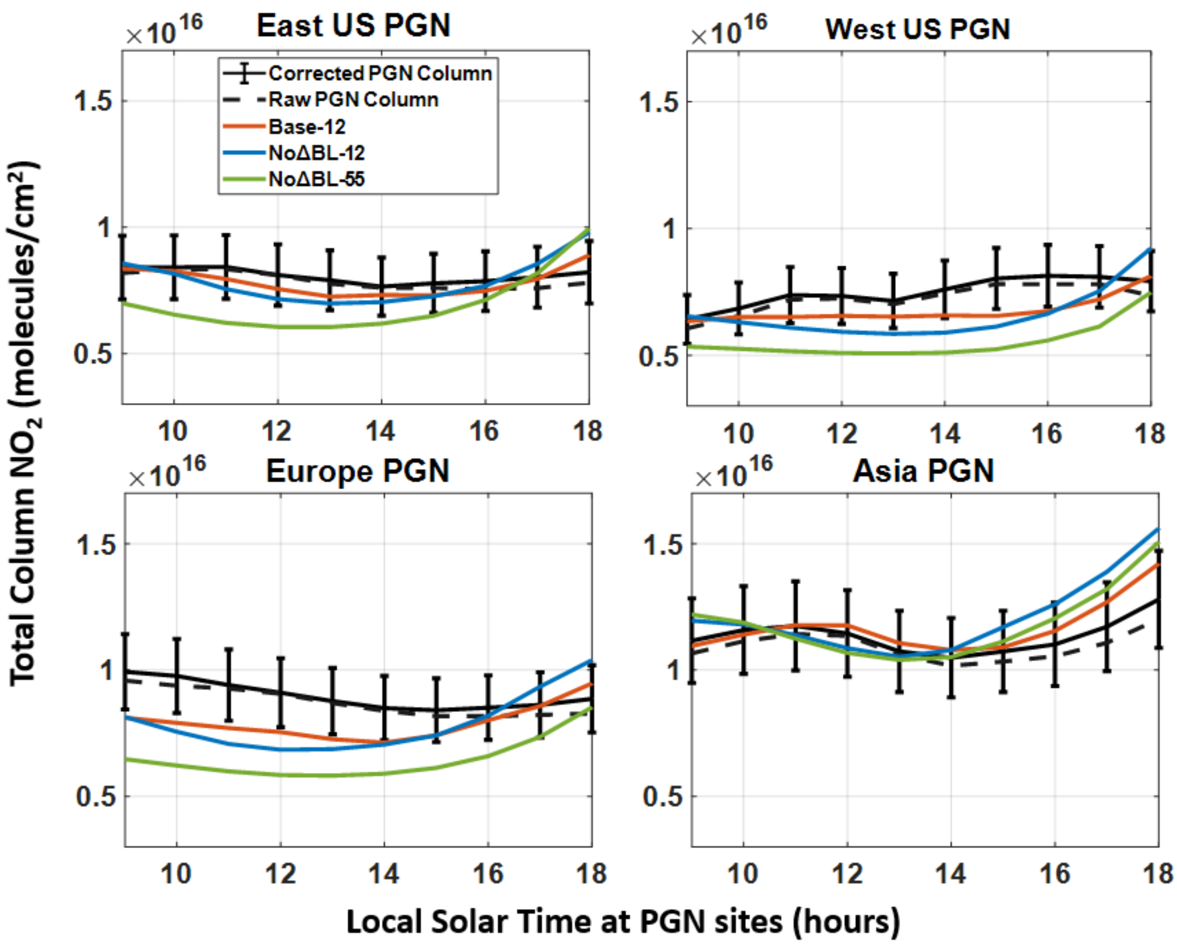

Figure 5. The total NO_2 vertical columns from corrected Pandora columns (black), raw Pandora columns (black dotted), the 12 km base case simulation (red), 12 km without modified PBLH (blue) and 55 km without modified PBLH (green) sampled over PGN sites for the summer months of June-July-August in 2019. Error bars indicate standard error.

3.4 Simulated total NO_2 columns

Figure 6 shows the 12 km and 55 km simulated total NO_2 columns, for the summer months of June-July-August in 2019, between 9 AM and 6 PM (local solar time) over the CONUS. The overlaid circles show the PGN mean total NO_2 columns. The 12 km simulated NO_2 columns exhibit greater heterogeneity and better consistency with PGN observed columns (NB = 13%) as compared to the 55 km simulated NO_2 columns (NB = 20%). This is primarily driven by better representation of emission and chemical processes at fine resolution (Zhang et al., 2023; Li et al., 2023a). Emissions at these sites are dominated by the transportation sector (Table A3). Figure 7

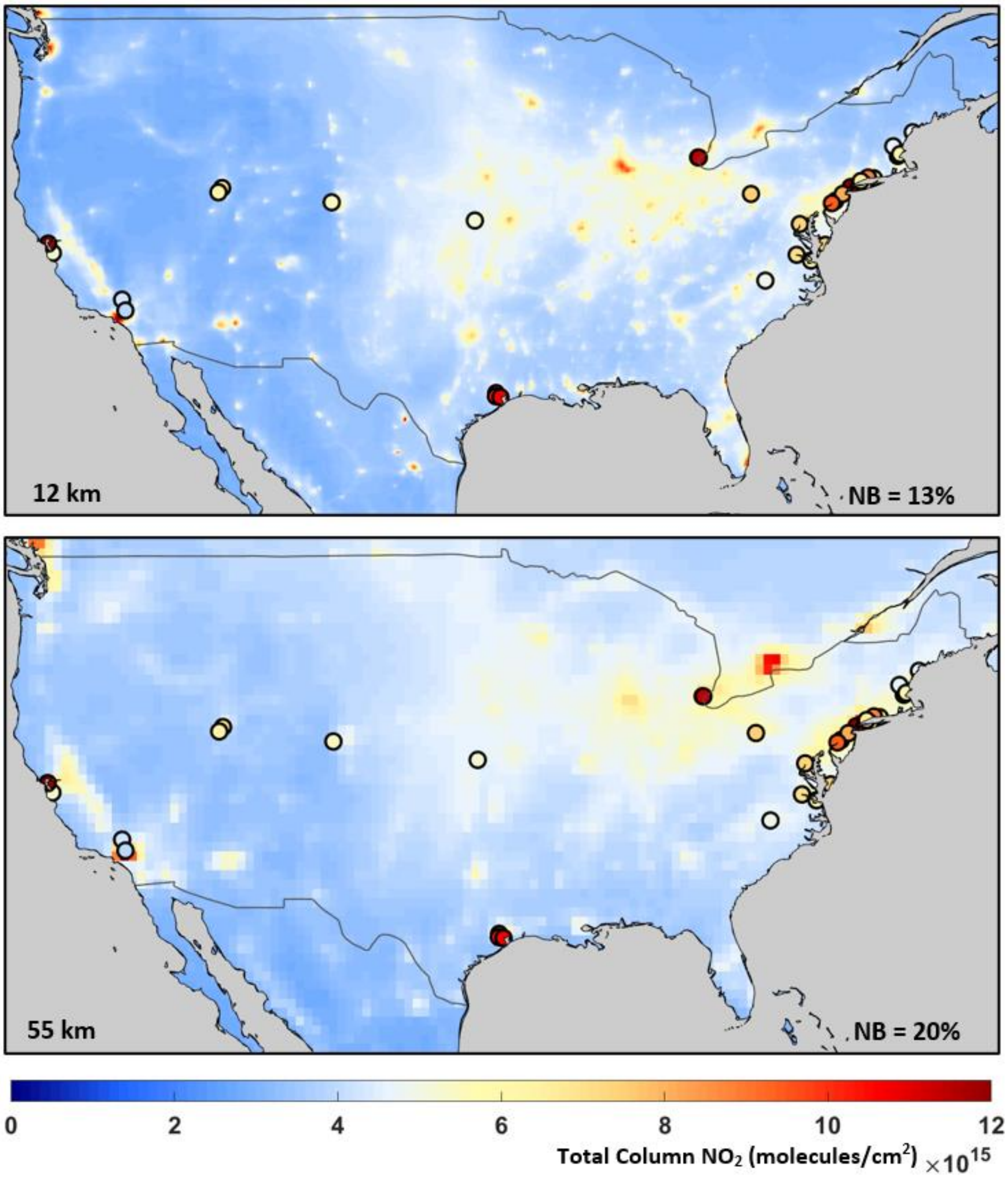

Figure 6. Simulated NO_2 total columns at 12 km (panel A) and 55 km (panel B) horizontal resolutions for the three-month average of June-July-August 2019 over domains where PGN monitors were available between 9 AM – 6 PM local solar time. The solid circles represent the PGN mean total columns between 9 AM – 6 PM local solar time for PGN sites in CONUS (31)

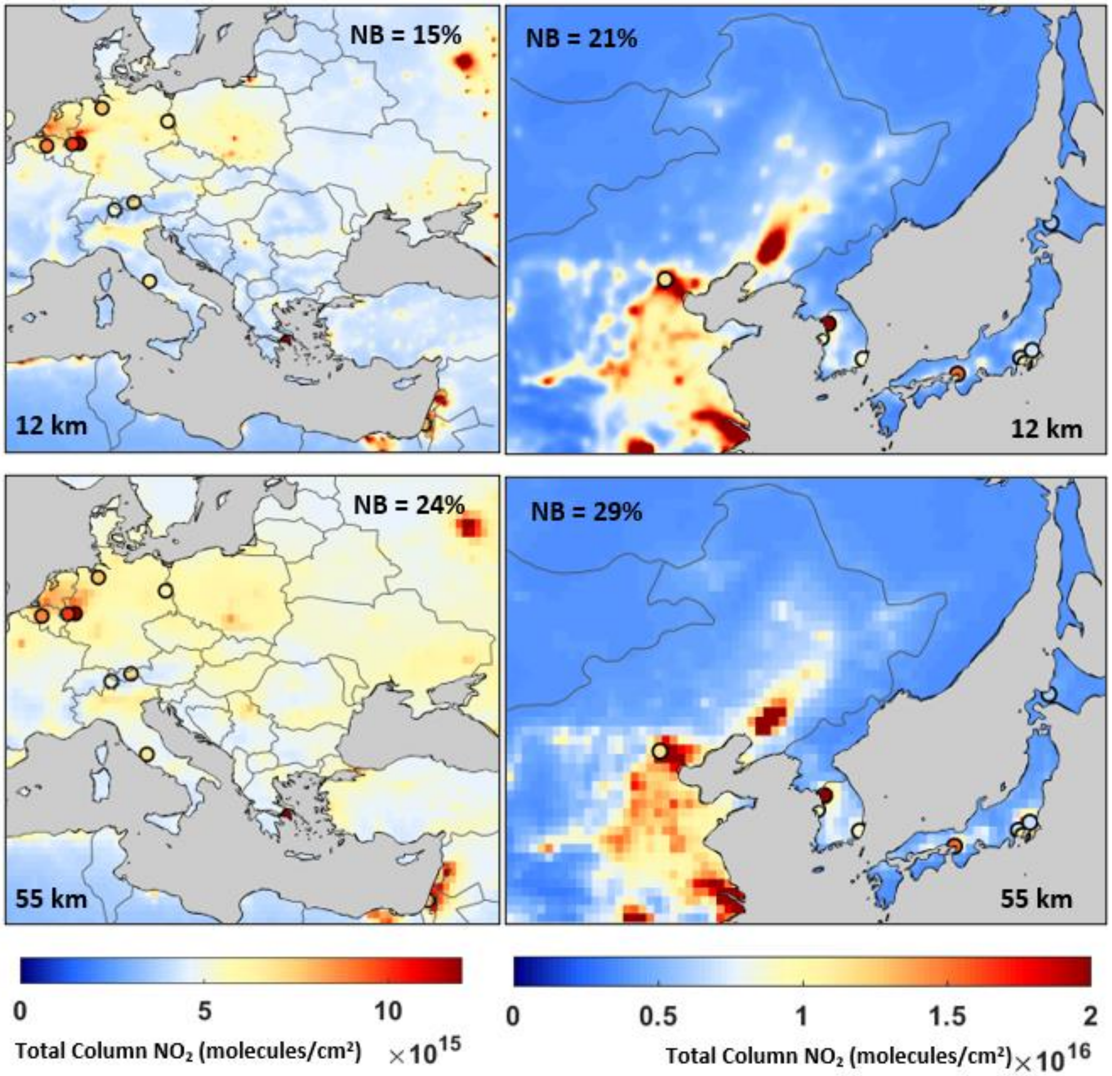

Figure 7. Simulated NO_2 total columns at 12 km (panel C and D) and 55 km (panel E and F) horizontal resolutions for the three-month average of June-July-August 2019 over domains where PGN monitors were available between 9 AM – 6 PM local solar time. The solid circles represent the PGN mean total columns between 9 AM – 6 PM local solar time for the PGN sites in Europe (10) and Asia (9).

shows the total NO_2 columns from PGN, 12 km simulation and 55 km simulation for the summer months of June-July- August in 2019, between 9 AM and 6 PM local solar time over Europe and East Asia. We find enhanced NO_2 vertical columns over urban areas in western Europe, eastern China, Japan and the Korean peninsula. The 12 km simulated NO_2 columns exhibit more resolved combustion features and better agreement with Pandora observed columns for Europe (NB = 15%) and east Asia (NB = 17%) as compared to the 55 km simulated NO_2 columns for Europe (NB =

24%) and east Asia (NB = 29%).

3.5 Hourly variation of observed and simulated surface NO_2 concentrations

Figure 8 shows the hourly variation in surface NO_2 mixing ratios from the corrected in situ measurements and 12 km simulations over Maryland, Texas and Colorado. Measured NO_2 mixing ratios are greater in morning and evening than in afternoon as expected from the mixed layer growth and shorter NO_x lifetime in afternoon. Observed NO_2 surface concentrations over PGN sites in Asia show enhancement at evening hours (5-6 PM) as compared to PGN sites elsewhere.

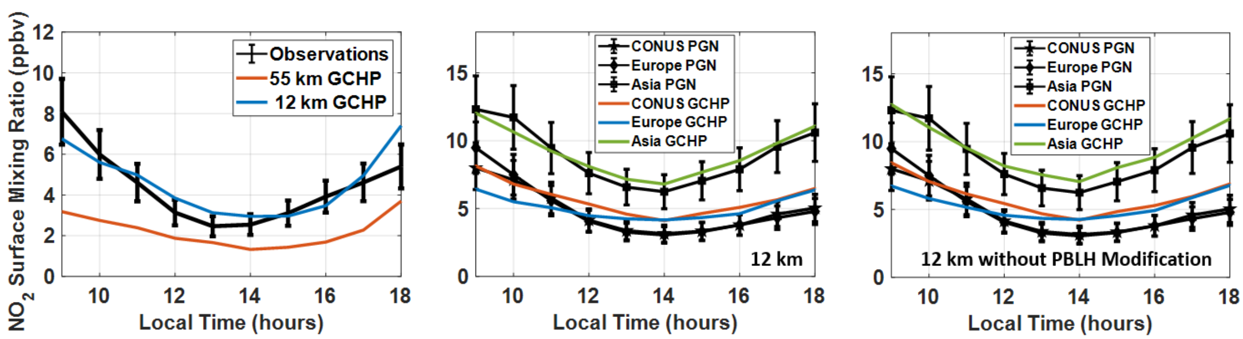

Figure 8. The left panel shows the hourly variation of corrected surface NO_2 mixing ratios from observations during the DISCOVER-AQ campaign. The middle and right panels show the hourly variation of observed and 12 km simulated surface NO_2 mixing ratios averaged over the PGN sites with and without PBLH modification respectively. Error bars indicate standard error.

The measurements are better represented at 12 km (NB = 21%) than at 55 km (NB = 63%) by better resolving high NO_x emissions near measurement sites. Both Base_12 and NoΔBL_12 simulated NO_2 concentrations generally represent the observations well with NB = 18% (Base_12) and NB = 20% (NoΔBL_12), across all PGN sites.

3.6 Hourly variation of layer contributions to simulated total NO_2 columns

Given the overall skill of the 12 km simulations in representing the Pandora, aircraft, and surface NO_2 we proceed to apply the 12 km simulations to understand how the simulated NO_2 vertical profile affects the simulated NO_2 column to surface relationship. Figure 9 shows the hourly variation of simulated contributions to the NO_2 total columns (Base_12) from different vertical layers for multiple regions. In all four regions, within the troposphere, the layer below 0.5 km is the largest contributor at 9 AM with a diminishing contribution into the afternoon associated with mixed layer growth followed by an increasing contribution towards evening. The contribution

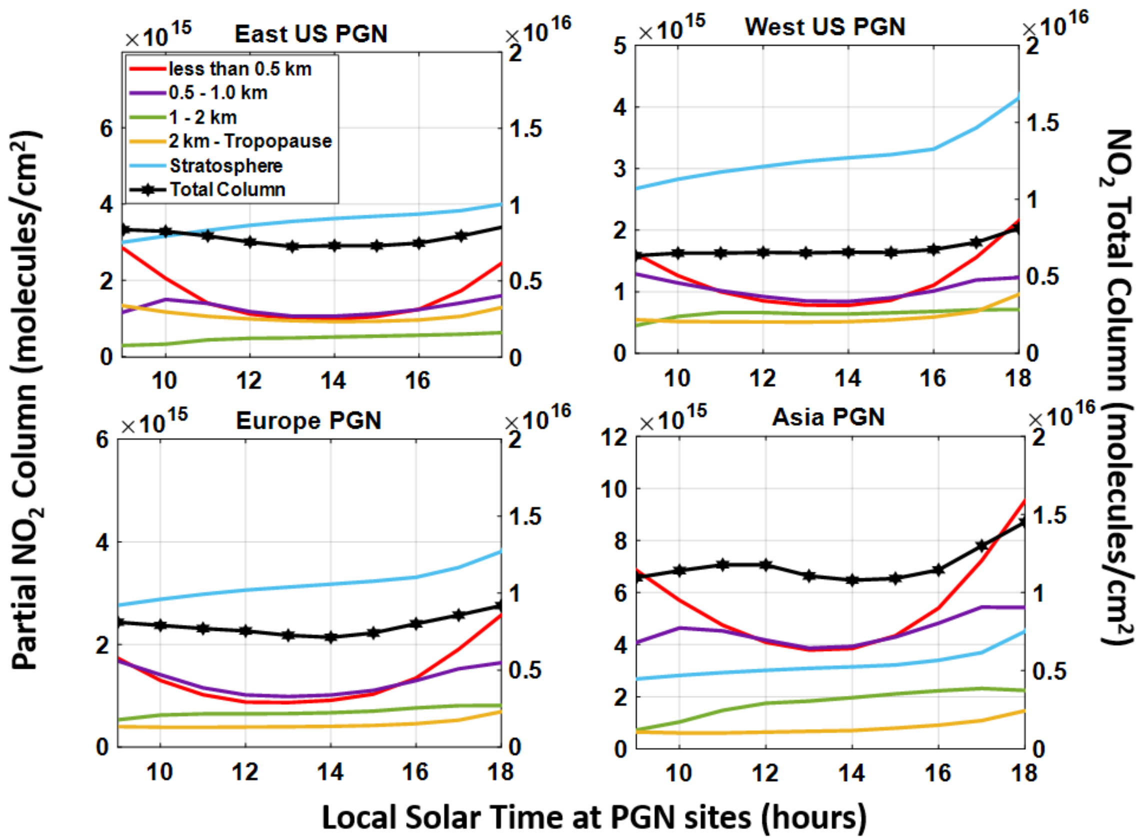

Figure 9. The simulated absolute contribution of NO_2 columns at different hours of the day averaged over the summer months of June-July-August for 2019 for PGN sites over the eastern US, western US, Europe, and eastern Asia. The colored lines resemble the absolute concentrations from different sections of the column. The black line (hexagon) represents the total NO_2 column. The right y-axis (specifically for the total NO_2 column representing the black marked line) shows the total columns of NO_2.

from layers between 0.5 km and the tropopause has weaker variation contributing to the overall weaker variation in total columns. Fractional layer contributions are shown in Figure A8. Fractional hourly variation of the layers above 0.5 km exhibits a compensating inverse behavior, with a pronounced variation in the stratospheric fraction. Contributions from the free troposphere are relatively high for the eastern US reflecting the lightning contribution (Shah et al., 2023; Dang et al., 2023). Over Asia the fractional contribution below 0.5 km is the highest (26% - 42%) reflecting major surface contributions. Overall, we find that for all four regions, the hourly variation in the total column reflects hourly variation below 500 m, dampened by greater column contributions above 500 m that dominate the total column.

Conclusion

We applied GCHP to investigate the hourly variation of summertime NO_2 columns and surface concentrations by interpreting DISCOVER-AQ aircraft and ground-based measurements over Maryland, Texas, Colorado and PGN measurements over the CONUS, Europe, and eastern Asia. We corrected the hourly variation in Pandora observations for the effects of temperature on the NO_2 cross section and the local solar time along the Pandora line-of-sight. The site-specific effective temperature correction factors typically increase the hourly variation of the Pandora observed columns over DISCOVER_AQ sites (3.5% from the daytime mean) and PGN sites (4% from the daytime mean). Near sunrise and sunset, differences in local solar time observed by Pandora in the stratosphere versus the measurement site reflect displacement of 5-10 mins in local solar time toward noon which is relevant in the stratosphere near sunrise and sunset when the NO_2/NO_x ratio is varying rapidly. These corrections to the Pandora measurements improve their consistency with the hourly variation in the NO_2 columns inferred from DISCOVER-AQ aircraft measurements. We find that fine scale simulations at 12 km better represent the NO_2 vertical profile measured by aircraft, reducing the NB from 23% to 16% as compared to simulations at a moderate resolution of 55 km. Simulations at fine resolution (~12 km) of vertical columns along the line-of-sight of Pandora instruments have lower NB with Pandora sun photometers at DISCOVER-AQ sites (10%), and across the eastern US (9%), western US (14%), Europe (15%) and Asia (21%) as compared to moderate resolution (55 km). Fine resolution represents atmospheric physical and chemical processes with greater accuracy. Excluding the effects of model resolution and the PBLH modification increases the NB to 21% across DISCOVER-AQ sites (over Maryland, Texas and Colorado) and increases the NB at PGN sites over the eastern US (17%), western US (24%), Europe (24%) and east Asia (29%). Adjusting the PBLH to represent observations improves the daytime variation in NO_2/NO_x ratios by increasing the NO_2/NO_x ratio in midday and decreasing the NO_2/NO_x ratio in the afternoon and evening.

Our study highlights the importance of fine scale total NO_2 columns (troposphere and stratosphere) to interpret the hourly variation of NO_2 column-to-surface relationships, as compared to tropospheric columns exclusively described in prior studies. Given the overall skill of the 12 km GCHP simulations in representing the corrected Pandora, aircraft, and surface NO_2 measurements, we apply them to derive the hourly contribution of vertical layers to the total tropospheric columns. We find weaker hourly variation in total NO_2 columns than in the lowest 500 m where NO_2 concentrations are greater in morning and evening than midday, while the residual tropospheric column above 500 m dominates the total column with weaker variability. Thus, the weak hourly variation in the column reflects fractional contributions from NO_2 below and above 500 m.

Despite the skill of the 12 km simulations in representing the Pandora column measurements, there appears to be greater hourly variation in the simulation, the aircraft measurements, and the surface measurements than in the Pandora observations. Future work should continue to understand this relationship. Future work should also leverage the information developed here to test the performance of surface NO_2 concentrations inferred from the geostationary constellation against ground-based measurements.

Code and Data Availability

GEOS-Chem 14.1.1 along with GCHP code is available for download at https://github.com/geoschem/GCHP.git. The PGN data is available at https://data.pandonia-global-network.org/. The DISCOVER-AQ aircraft and Pandora data are available here: https://asdc.larc.nasa.gov/project/DISCOVER-AQ. For hourly simulated NO_2 datasets please contact the author (deepangsuchatterjee@wustl.edu; deepangsuchatterjee@gmail.com)

Author contributions

The manuscript was written using contributions from all authors. The conceptualization was initialized by DC and RVM. The methodology was developed by DC and RVM .DC conducted the model simulations. DC conducted the data analysis with help from CL,DZ,HZ,LL,DH,RC. JC conducted the DISCOVER-AQ campaign. AC manages the PGN datasets. DC and RVM wrote the original draft. All authors have reviewed, edited and given approval to the final version of the manuscript.

Competing interests

The contact author has declared that neither they nor their co-authors have any competing interests.

Acknowledgments

This work has been supported by the NASA Grant 80NSSC21K1343 and 80NSSC21K0508 and NSF Grant 2244984. We thank the GEOS-Chem support team for maintaining the model used in this work.

Reference

Al-Saadi, J., Kim, J., Lambert, J.-C., Veihelmann, B., and Chance, K.: Geostationary Satellite Constellation for Observing Global Air Quality : Geophysical Validation Needs, 2017.

Anenberg, S. C., Henze, D. K., Tinney, V., Kinney, P. L., Raich, W., Fann, N., Malley, C. S., Roman, H., Lamsal, L., Duncan, B., Martin, R. V., van Donkelaar, A., Brauer, M., Doherty, R., Jonson, J. E., Davila, Y., Sudo, K., and Kuylenstierna, J. C. I.: Estimates of the global burden of ambient PM2:5, ozone, and NO2 on asthma incidence and emergency room visits, Environ. Health Perspect., 126, 1–14, https://doi.org/10.1289/EHP3766, 2018.

Anenberg, S. C., Mohegh, A., Goldberg, D. L., Kerr, G. H., Brauer, M., Burkart, K., Hystad, P., Larkin, A., Wozniak, S., and Lamsal, L.: Long-term trends in urban NO2 concentrations and associated paediatric asthma incidence: estimates from global datasets, Lancet Planet. Heal., 6, e49–e58, https://doi.org/10.1016/S2542-5196(21)00255-2, 2022.

Bates, K. H. and Jacob, D. J.: A new model mechanism for atmospheric oxidation of isoprene: Global effects on oxidants, nitrogen oxides, organic products, and secondary organic aerosol, Atmos. Chem. Phys., 19, 9613–9640, https://doi.org/10.5194/acp-19-9613-2019, 2019.

Bates, K. H., Jacob, D. J., Li, K., Ivatt, P. D., Evans, M. J., Yan, Y., and Lin, J.: Development and evaluation of a new compact mechanism for aromatic oxidation in atmospheric models, Atmos. Chem. Phys., 21, 18351–18374, https://doi.org/10.5194/acp-21-18351-2021, 2021.

Bauer, S. E., Koch, D., Unger, N., Metzger, S. M., Shindell, D. T., and Streets, D. G.: Nitrate aerosols today and in 2030: A global simulation including aerosols and tropospheric ozone, Atmos. Chem. Phys., 7, 5043–5059, https://doi.org/10.5194/acp-7-5043-2007, 2007.

Belinha, J.: Manual for FEMAS Manual for FEMAS, 1–83, 2016.

Bindle, L., Martin, R. V., Cooper, M. J., Lundgren, E. W., Eastham, S. D., Auer, B. M., Clune, T. L., Weng, H., Lin, J., Murray, L. T., Meng, J., Keller, C. A., Putman, W. M., Pawson, S., and Jacob, D. J.: Grid-stretching capability for the GEOS-Chem 13.0.0 atmospheric chemistry model, Geosci. Model Dev., 14, 5977–5997, https://doi.org/10.5194/GMD-14-5977-2021, 2021.

Burnett, R. T., Stieb, D., Brook, J. R., Cakmak, S., Dales, R., Raizenne, M., Vincent, R., and Dann, T.: Associations between Short-Term Changes in Nitrogen Dioxide and Mortality in Canadian Cities, Arch. Environ. Heal. An Int. J., 59, 228–236, https://doi.org/10.3200/AEOH.59.5.228-236, 2004.

Cede (2021) https://www.pandonia-global-network.org/wpcontent/uploads/2021/09/BlickSoftwareSuite_Manual_v1-8-4.pdf

Choi, S., Lamsal, L. N., Follette-Cook, M., Joiner, J., Krotkov, N. A., Swartz, W. H., Pickering, K. E., Loughner, C. P., Appel, W., Pfister, G., Saide, P. E., Cohen, R. C., Weinheimer, A. J., and Herman, J. R.: Assessment of NO2 observations during DISCOVER-AQ and KORUS-AQ field campaigns, Atmos. Meas. Tech., 13, 2523–2546, https://doi.org/10.5194/amt-13-2523-2020, 2020.

Cooper, M. J., Martin, R. V., Hammer, M. S., Levelt, P. F., Veefkind, P., Lamsal, L. N., Krotkov, N. A., Brook, J. R., and McLinden, C. A.: Global fine-scale changes in ambient NO2 during COVID-19 lockdowns, Nature, 601, 380–387, https://doi.org/10.1038/s41586-021-04229-0, 2022.

Crawford, J. H., Ahn, J., Al-saadi, J., Chang, L., Emmons, L. K., Kim, J., Lee, G., Park, J., Park, R. J., Woo, J. H., Song, C., Hong, J., Hong, Y., Lefer, B. L., Lee, M., Lee, T., Kim, S., Min, K., Yum, S. S., Shin, H. J., Kim, Y., Choi, J., Park, J., Szykman, J. J., Long, R. W., Jordan, C. E., Simpson, I. J., Fried, A., Dibb, J. E., Cho, S., and Kim, Y. P.: The Korea-United States Air Quality (KORUS-AQ) field study, 1–27, 2021.

Crippa, M., Guizzardi, D., Muntean, M., Schaaf, E., Dentener, F., Van Aardenne, J. A., Monni, S., Doering, U., Olivier, J. G. J., Pagliari, V., and Janssens-Maenhout, G.: Gridded emissions of air pollutants for the period 1970-2012 within EDGAR v4.3.2, Earth Syst. Sci. Data, 10, 1987–2013, https://doi.org/10.5194/essd-10-1987-2018, 2018.

Dang, R., Jacob, D. J., Shah, V., Eastham, S. D., Fritz, T. M., Mickley, L. J., Liu, T., Wang, Y., and

Wang, J.: Background nitrogen dioxide (NO2) over the United States and its implications for satellite observations and trends: effects of nitrate photolysis, aircraft, and open fires, Atmos. Chem. Phys., 23, 6271–6284, https://doi.org/10.5194/acp-23-6271-2023, 2023.

David, L. M. and Nair, P. R.: Diurnal and seasonal variability of surface ozone and NO x at a tropical coastal site: Association with mesoscale and synoptic meteorological conditions , J. Geophys. Res., 116, 1–16, https://doi.org/10.1029/2010jd015076, 2011.

Day, D. A., Wooldridge, P. J., Dillon, M. B., Thornton, J. A., and Cohen, R. C.: A thermal dissociation laser-induced fluorescence instrument for in situ detection NO2, peroxy nitrates, alkyl nitrates, and HNO3, J. Geophys. Res. Atmos., 107, https://doi.org/10.1029/2001jd000779, 2002.

Day, D. A., Farmer, D. K., Goldstein, A. H., Wooldridge, P. J., Minejima, C., and Cohen, R. C.: Observations of NOx, σpNs, σaNs, and HNO3 at a rural site in the California Sierra Nevada Mountains: Summertime diurnal cycles, Atmos. Chem. Phys., 9, 4879–4896, https://doi.org/10.5194/acp-9-4879-2009, 2009.

Duncan, B. N., Yoshida, Y., De Foy, B., Lamsal, L. N., Streets, D. G., Lu, Z., Pickering, K. E., and Krotkov, N. A.: The observed response of Ozone Monitoring Instrument (OMI) NO2 columns to NOx emission controls on power plants in the United States: 2005-2011, Atmos. Environ., 81, 102–111, https://doi.org/10.1016/j.atmosenv.2013.08.068, 2013.

Eastham, S. D., Weisenstein, D. K., and Barrett, S. R. H.: Development and evaluation of the unified tropospheric-stratospheric chemistry extension (UCX) for the global chemistry-transport model GEOS-Chem, Atmos. Environ., 89, 52–63, https://doi.org/10.1016/j.atmosenv.2014.02.001, 2014.

Eastham, S. D., Long, M. S., Keller, C. A., Lundgren, E., Yantosca, R. M., Zhuang, J., Li, C., Lee, C. J., Yannetti, M., Auer, B. M., Clune, T. L., Kouatchou, J., Putman, W. M., Thompson, M. A., Trayanov, A. L., Molod, A. M., Martin, R. V., and Jacob, D. J.: GEOS-Chem high performance (GCHP v11-02c): A next-generation implementation of the GEOS-Chem chemical transport model for massively parallel applications, Geosci. Model Dev., 11, 2941–2953, https://doi.org/10.5194/GMD-11-2941-2018, 2018.

Flynn, C. M., Pickering, K. E., Crawford, J. H., Lamsal, L., Krotkov, N., Herman, J., Weinheimer, A., Chen, G., Liu, X., Szykman, J., Tsay, S. C., Loughner, C., Hains, J., Lee, P., Dickerson, R. R., Stehr, J. W., and Brent, L.: Relationship between column-density and surface mixing ratio: Statistical analysis of O3 and NO2 data from the July 2011 Maryland DISCOVER-AQ mission, Atmos. Environ., 92, 429–441, https://doi.org/10.1016/j.atmosenv.2014.04.041, 2014.

Fountoukis, C. and Nenes, A.: ISORROPIAII: A computationally efficient thermodynamic equilibrium model for K+-Ca2+-Mg2+-NH4+-Na+-SO42--NO3--Cl--H2O aerosols, Atmos. Chem. Phys., 7, 4639–4659, https://doi.org/10.5194/ACP-7-4639-2007, 2007.

Geddes, J. A. and Martin, R. V: Global deposition of total reactive nitrogen oxides from, Atmos. Chem. Phys., 17, 10071–10091, 2017.

Ghude, S. D., Karumuri, R. K., Jena, C., Kulkarni, R., Pfister, G. G., Sajjan, V. S., Pithani, P., Debnath, S., Kumar, R., Upendra, B., Kulkarni, S. H., Lal, D. M., Vander A, R. J., and Mahajan, A. S.: What is driving the diurnal variation in tropospheric NO2 columns over a cluster of high emission thermal power plants in India?, Atmos. Environ. X, 5, 100058, https://doi.org/10.1016/j.aeaoa.2019.100058, 2020.

Herman, J., Cede, A., Spinei, E., Mount, G., Tzortziou, M., and Abuhassan, N.: NO2 column amounts from ground-based Pandora and MFDOAS spectrometers using the direct-sun DOAS technique: Intercomparisons and application to OMI validation, J. Geophys. Res. Atmos., 114, 1–20, https://doi.org/10.1029/2009jd011848, 2009.

Herman, J., Evans, R., Cede, A., Abuhassan, N., Petropavlovskikh, I., and McConville, G.: Comparison of ozone retrievals from the Pandora spectrometer system and Dobson spectrophotometer in Boulder, Colorado, Atmos. Meas. Tech., 8, 3407–3418, https://doi.org/10.5194/amt-8-3407-2015, 2015.

Holmes, C. D., Bertram, T. H., Confer, K. L., Graham, K. A., Ronan, A. C., Wirks, C. K., and Shah, V.: The Role of Clouds in the Tropospheric NOx Cycle: A New Modeling Approach for Cloud Chemistry and Its Global Implications, Geophys. Res. Lett., 46, 4980–4990, https://doi.org/10.1029/2019GL081990, 2019.

Hu, L., Keller, C. A., Long, M. S., Sherwen, T., Auer, B., Da Silva, A., Nielsen, J. E., Pawson, S., Thompson, M. A., Trayanov, A. L., Travis, K. R., Grange, S. K., Evans, M. J., and Jacob, D. J.: Global simulation of tropospheric chemistry at 12.5 km resolution: Performance and evaluation of the GEOS-Chem chemical module (v10-1) within the NASA GEOS Earth system model (GEOS-5 ESM), Geosci. Model Dev., 11, 4603–4620, https://doi.org/10.5194/gmd-11-4603-2018, 2018.

Jacob, D. J., Heikes, B. G., Fan, S. M., Logan, J. A., Mauzerall, D. L., Bradshaw, J. D., Singh, H. B., Gregory, G. L., Talbot, R. W., Blake, D. R., and Sachse, G. W.: Origin of ozone and NOx in the tropical troposphere: A photochemical analysis of aircraft observations over the South Atlantic basin, J. Geophys. Res. Atmos., 101, 24235–24250, https://doi.org/10.1029/96jd00336, 1996.

L Laughner, J., Zhu, Q., and Cohen, R. C.: Evaluation of version 3.0B of the BEHR OMI NO2 product, Atmos. Meas. Tech., 12, 128–146, https://doi.org/10.5194/amt-12-129-2019, 2019.

Lamsal, L. N., Martin, R. V., van Donkelaar, A., Steinbacher, M., Celarier, E. A., Bucsela, E., Dunlea, E. J., and Pinto, J. P.: Ground-level nitrogen dioxide concentrations inferred from the satellite-borne Ozone Monitoring Instrument, J. Geophys. Res. Atmos., 113, 1–15, https://doi.org/10.1029/2007JD009235, 2008.

Lamsal, L. N., Martin, R. V., Padmanabhan, A., Van Donkelaar, A., Zhang, Q., Sioris, C. E., Chance, K., Kurosu, T. P., and Newchurch, M. J.: Application of satellite observations for timely updates to global anthropogenic NOx emission inventories, Geophys. Res. Lett., 38, https://doi.org/10.1029/2010GL046476, 2011.

Laughner, J. and Cohen, R. C.: Direct observation of changing NO, Science (80-.)., 366, 723–727, 2019.

Laughner, J. L., Zhu, Q., and Cohen, R. C.: The Berkeley High Resolution Tropospheric NO2 product, Earth Syst. Sci. Data, 10, 2069–2095, https://doi.org/10.5194/essd-10-2069-2018, 2018.

Li, C., Martin, R. V., Cohen, R. C., Bindle, L., Zhang, D., Chatterjee, D., Weng, H., and Lin, J.: Variable effects of spatial resolution on modeling of nitrogen oxides, Atmos. Chem. Phys., 23, 3031–3049, https://doi.org/10.5194/acp-23-3031-2023, 2023a.

Li, J., Wang, Y., Zhang, R., Smeltzer, C., Weinheimer, A., Herman, J., Boersma, K. F., Celarier, E. A., Long, R. W., Szykman, J. J., Delgado, R., Thompson, A. M., Knepp, T. N., Lamsal, L. N., Janz, S. J., Kowalewski, M. G., Liu, X., and Nowlan, C. R.: Comprehensive evaluations of diurnal NO2 measurements during DISCOVER-AQ 2011: Effects of resolution-dependent representation of NOx emissions, Atmos. Chem. Phys., 21, 11133–11160, https://doi.org/10.5194/acp-21-11133-2021, 2021.

Li, Y., Martin, R. V., Li, C., Boys, B. L., van Donkelaar, A., Meng, J., and Pierce, J. R.: Development and evaluation of processes affecting simulation of diel fine particulate matter variation in the GEOS-Chem model, Atmos. Chem. Phys., 23, 12525–12543, https://doi.org/10.5194/acp-23-12525-2023, 2023b.

Lin, J. T. and McElroy, M. B.: Impacts of boundary layer mixing on pollutant vertical profiles in the lower troposphere: Implications to satellite remote sensing, Atmos. Environ., 44, 1726–1739, https://doi.org/10.1016/j.atmosenv.2010.02.009, 2010.

GMDD - Improved Advection, Resolution, Performance, and Community Access in the New Generation (Version 13) of the High Performance GEOS-Chem Global Atmospheric Chemistry Model (GCHP): https://gmd.copernicus.org/preprints/gmd-2022-42/, last access: 18 June 2022.

Millet, D. B., Baasandorj, M., Farmer, D. K., Thornton, J. A., Baumann, K., Brophy, P., Chaliyakunnel, S., De Gouw, J. A., Graus, M., Hu, L., Koss, A., Lee, B. H., Lopez-Hilfiker, F. D., Neuman, J. A., Paulot, F., Peischl, J., Pollack, I. B., Ryerson, T. B., Warneke, C., Williams, B. J., and Xu, J.: A large and ubiquitous source of atmospheric formic acid, Atmos. Chem. Phys., 15, 6283–6304, https://doi.org/10.5194/acp-15-6283-2015, 2015.

Murray, L. T., Jacob, D. J., Logan, J. A., Hudman, R. C., and Koshak, W. J.: Optimized regional and interannual variability of lightning in a global chemical transport model constrained by LIS/OTD satellite data, J. Geophys. Res. Atmos., 117, 1–14, https://doi.org/10.1029/2012JD017934, 2012.

Nault, B. A., Garland, C., Pusede, S. E., Wooldridge, P. J., Ullmann, K., Hall, S. R., and Cohen, R. C.: Measurements of CH3O2NO2 in the upper troposphere, Atmos. Meas. Tech., 8, 987–997, https://doi.org/10.5194/amt-8-987-2015, 2015.

Oak, Y. J., Park, R. J., Schroeder, J. R., Crawford, J. H., Blake, D. R., Weinheimer, A. J., Woo, J. H., Kim, S. W., Yeo, H., Fried, A., Wisthaler, A., and Brune, W. H.: Evaluation of simulated O3 production efficiency during the KORUS-AQ campaign: Implications for anthropogenic NOx emissions in Korea, Elementa, 7, https://doi.org/10.1525/elementa.394, 2019.

Reed, A. J., Thompson, A. M., Kollonige, D. E., Martins, D. K., Tzortziou, M. A., Herman, J. R., Berkoff, T. A., Abuhassan, N. K., and Cede, A.: Effects of local meteorology and aerosols on ozone and nitrogen dioxide retrievals from OMI and pandora spectrometers in Maryland, USA during DISCOVER-AQ 2011, J. Atmos. Chem., 72, 455–482, https://doi.org/10.1007/s10874-013-9254-9, 2015.

Russell, A. R., Perring, A. E., Valin, L. C., Bucsela, E. J., Browne, E. C., Wooldridge, P. J., and Cohen, R. C.: A high spatial resolution retrieval of NO2 column densities from OMI: Method and evaluation, Atmos. Chem. Phys., 11, 8543–8554, https://doi.org/10.5194/acp-11-8543-2011, 2011.

Shah, V., J. Jacob, D., Li, K., Silvern, R., Zhai, S., Liu, M., Lin, J., and Zhang, Q.: Effect of changing NO*x* lifetime on the seasonality and long-term trends of satellite-observed tropospheric NO2 columns over China, Atmos. Chem. Phys., 20, 1483–1495, https://doi.org/10.5194/acp-20-1483-2020, 2020.

Shah, V., Jacob, D. J., Dang, R., Lamsal, L. N., Strode, S. A., Steenrod, S. D., Boersma, K. F., Eastham, S. D., Fritz, T. M., Thompson, C., Peischl, J., Bourgeois, I., Pollack, I. B., Nault, B. A., Cohen, R. C., Campuzano-Jost, P., Jimenez, J. L., Andersen, S. T., Carpenter, L. J., Sherwen, T., and Evans, M. J.: Nitrogen oxides in the free troposphere: Implications for tropospheric oxidants and the interpretation of satellite NO2 measurements, Atmos. Chem. Phys., 23, 1227–1257, https://doi.org/10.5194/acp-23-1227-2023, 2023.

Simone, N. W., Stettler, M. E. J., and Barrett, S. R. H.: Rapid estimation of global civil aviation emissions with uncertainty quantification, Transp. Res. Part D Transp. Environ., 25, 33–41, https://doi.org/10.1016/j.trd.2013.07.001, 2013.

Van Stratum, B. J. H., Vilá-Guerau De Arellano, J., Ouwersloot, H. G., Van Den Dries, K., Van Laar, T. W., Martinez, M., Lelieveld, J., Diesch, J. M., Drewnick, F., Fischer, H., Hosaynali Beygi, Z., Harder, H., Regelin, E., Sinha, V., Adame, J. A., Sörgel, M., Sander, R., Bozem, H., Song, W., Williams, J., and Yassaa, N.: Case study of the diurnal variability of chemically active species with respect to boundary layer dynamics during DOMINO, Atmos. Chem. Phys., 12, 5329–5341, https://doi.org/10.5194/acp-12-5329-2012, 2012.

Tao, Y., Huang, W., Huang, X., Zhong, L., Lu, S. E., Li, Y., Dai, L., Zhang, Y., and Zhu, T.: Estimated acute effects of ambient ozone and nitrogen dioxide on mortality in the Pearl River Delta of southern China, Environ. Health Perspect., 120, 393–398, https://doi.org/10.1289/ehp.1103715, 2012.

Thornton, J. A., Wooldridge, P. J., and Cohen, R. C.: Atmospheric NO2: In Situ laser-induced fluorescence detection at parts per trillion mixing ratios, Anal. Chem., 72, 528–539, https://doi.org/10.1021/ac9908905, 2000.

Tong, L., Zhang, H., Yu, J., He, M., Xu, N., Zhang, J., Qian, F., Feng, J., and Xiao, H.: Characteristics of surface ozone and nitrogen oxides at urban, suburban and rural sites in Ningbo, China, Atmos. Res., 187, 57–68, https://doi.org/10.1016/j.atmosres.2016.12.006, 2017.

Valin, L. C., Russell, A. R., Hudman, R. C., and Cohen, R. C.: Effects of model resolution on the interpretation of satellite NO2 observations, Atmos. Chem. Phys., 11, 11647–11655, https://doi.org/10.5194/acp-11-11647-2011, 2011.

Vandaele, A. C., Hermans, C., Fally, S., Carleer, M., Colin, R., Mérienne, M. F., Jenouvrier, A., and Coquart, B.: High-resolution Fourier transform measurement of the NO2 visible and near-infrared absorption cross sections: Temperature and pressure effects, J. Geophys. Res. Atmos., 107, ACH 3-1-ACH 3-12, https://doi.org/10.1029/2001JD000971, 2002.

Veefkind, J. P., Aben, I., McMullan, K., Förster, H., de Vries, J., Otter, G., Claas, J., Eskes, H. J., de Haan, J. F., Kleipool, Q., van Weele, M., Hasekamp, O., Hoogeveen, R., Landgraf, J., Snel, R., Tol, P., Ingmann, P., Voors, R., Kruizinga, B., Vink, R., Visser, H., and Levelt, P. F.: TROPOMI on the ESA Sentinel-5 Precursor: A GMES mission for global observations of the atmospheric composition for climate, air quality and ozone layer applications, Remote Sens. Environ., 120, 70–83, https://doi.org/10.1016/j.rse.2011.09.027, 2012.

Verhoelst, T., Compernolle, S., Pinardi, G., Lambert, J. C., Eskes, H. J., Eichmann, K. U., Fjæraa, A. M., Granville, J., Niemeijer, S., Cede, A., Tiefengraber, M., Hendrick, F., Pazmiño, A., Bais, A., Bazureau, A., Folkert Boersma, K., Bognar, K., Dehn, A., Donner, S., Elokhov, A., Gebetsberger, M., Goutail, F., Grutter De La Mora, M., Gruzdev, A., Gratsea, M., Hansen, G. H., Irie, H., Jepsen, N., Kanaya, Y., Karagkiozidis, D., Kivi, R., Kreher, K., Levelt, P. F., Liu, C., Müller, M., Navarro Comas, M., Piters, A. J. M., Pommereau, J. P., Portafaix, T., Prados-Roman, C., Puentedura, O., Querel, R., Remmers, J., Richter, A., Rimmer, J., Cárdenas, C. R., De Miguel, L. S., Sinyakov, V. P., Stremme, W., Strong, K., Van Roozendael, M., Pepijn Veefkind, J., Wagner, T., Wittrock, F., Yela González, M., and Zehner, C.: Ground-based validation of the Copernicus Sentinel-5P TROPOMI NO2 measurements with the NDACC ZSL-DOAS, MAX-DOAS and Pandonia global networks, Atmos. Meas. Tech., 14, 481–510, https://doi.org/10.5194/amt-14-481-2021, 2021.

Weng, H., Lin, J., Martin, R., Millet, D. B., Jaeglé, L., Ridley, D., Keller, C., Li, C., Du, M., and Meng, J.: Global high-resolution emissions of soil NOx, sea salt aerosols, and biogenic volatile organic compounds, Sci. Data, 7, 1–15, https://doi.org/10.1038/s41597-020-0488-5, 2020.

Yang, L. H., Jacob, D. J., Dang, R., Oak, Y. J., Lin, H., Kim, J., Zhai, S., Colombi, N. K., Pendergrass, D. C., Beaudry, E., Shah, V., Feng, X., Yantosca, R. M., Chong, H., Park, J., Lee, H., Lee, W.-J., Kim, S., Kim, E., Travis, K. R., Crawford, J. H., and Liao, H.: Interpreting GEMS geostationary satellite observations of the diurnal variation of nitrogen dioxide (NO_2) over East Asia, EGUsphere, 1–25, 2023a.

Yang, L. H., Jacob, D. J., Colombi, N. K., Zhai, S., Bates, K. H., Shah, V., Beaudry, E., Yantosca, R. M., Lin, H., Brewer, J. F., Chong, H., Travis, K. R., Crawford, J. H., Lamsal, L. N., Koo, J. H., and Kim, J.: Tropospheric NO2vertical profiles over South Korea and their relation to oxidant chemistry: implications for geostationary satellite retrievals and the observation of NO2diurnal variation from space, Atmos. Chem. Phys., 23, 2465–2481, https://doi.org/10.5194/acp-23-2465-2023, 2023b.

Zhang, D., Martin, R. V., Bindle, L., Li, C., Eastham, S. D., van Donkelaar, A., and Gallardo, L.: Advances in Simulating the Global Spatial Heterogeneity of Air Quality and Source Sector Contributions: Insights into the Global South, Environ. Sci. Technol., 57, 6955–6964, https://doi.org/10.1021/acs.est.2c07253, 2023.

Zhang, Y., Wang, Y., Chen, G., Smeltzer, C., Crawford, J., Olson, J., Szykman, J., Weinheimer, A. J., Knapp, D. J., Montzka, D. D., Wisthaler, A., Mikoviny, T., Fried, A., and Diskin, G.: Journal of Geophysical Research : Atmospheres of DISCOVER-AQ 2011 observations, 1–13, https://doi.org/10.1002/2015JD024203.Received, 2016.

Zhao, X., Fioletov, V., Cede, A., Davies, J., and Strong, K.: Accuracy, precision, and temperature dependence of Pandora total ozone measurements estimated from a comparison with the Brewer triad in Toronto, Atmos. Meas. Tech., 9, 5747–5761, https://doi.org/10.5194/amt-9-5747-2016, 2016.

Appendix

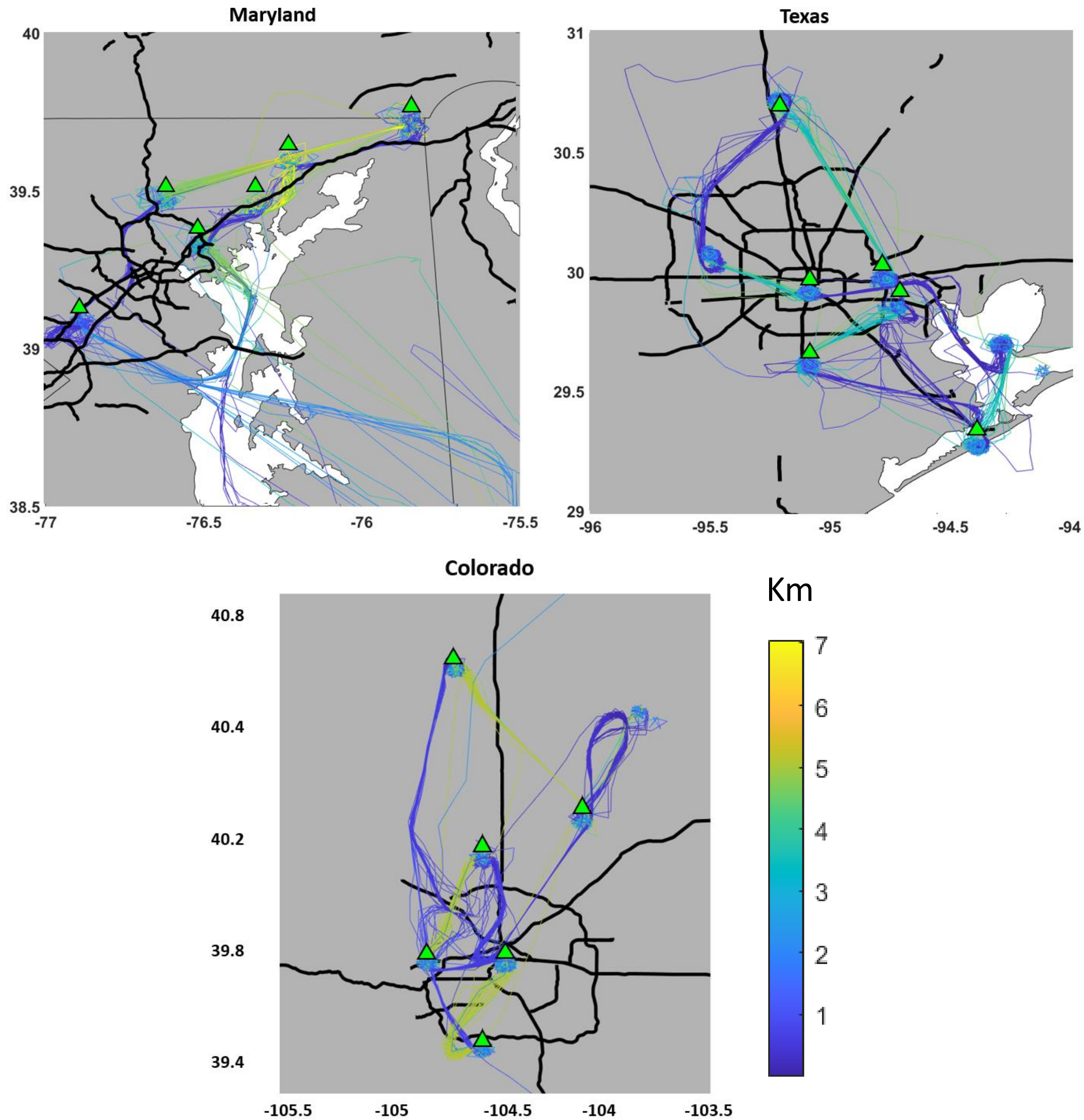

Figure A1. Flight tracks showing the path and altitude of the P-3B aircraft during the DISCOVER-AQ campaign over Maryland during July 2011 (left), over Texas during September 2013 (center) and over Colorado during July-August 2014 (right). The green triangles show the locations of the Pandora sun photometers that have been used in this study. The Sites names and coordinates are listed in Table A1. Grey indicates land, white indicates water. The black bold lines indicate roads.

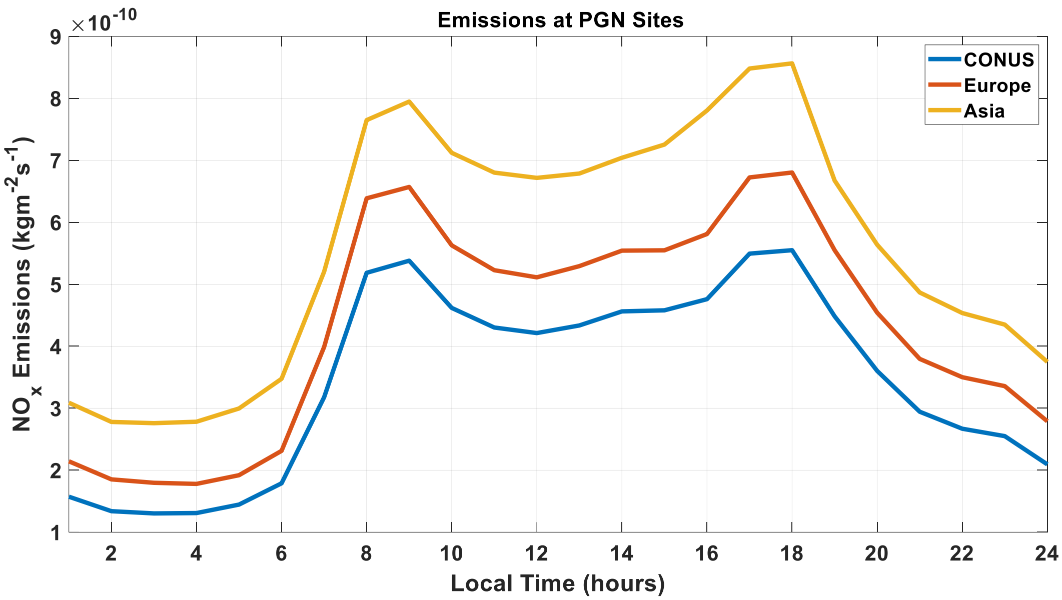

Figure A2. Hourly variation of NOx emissions including all sectors across 50 PGN sites over the CONUS, Europe, and east Asia.

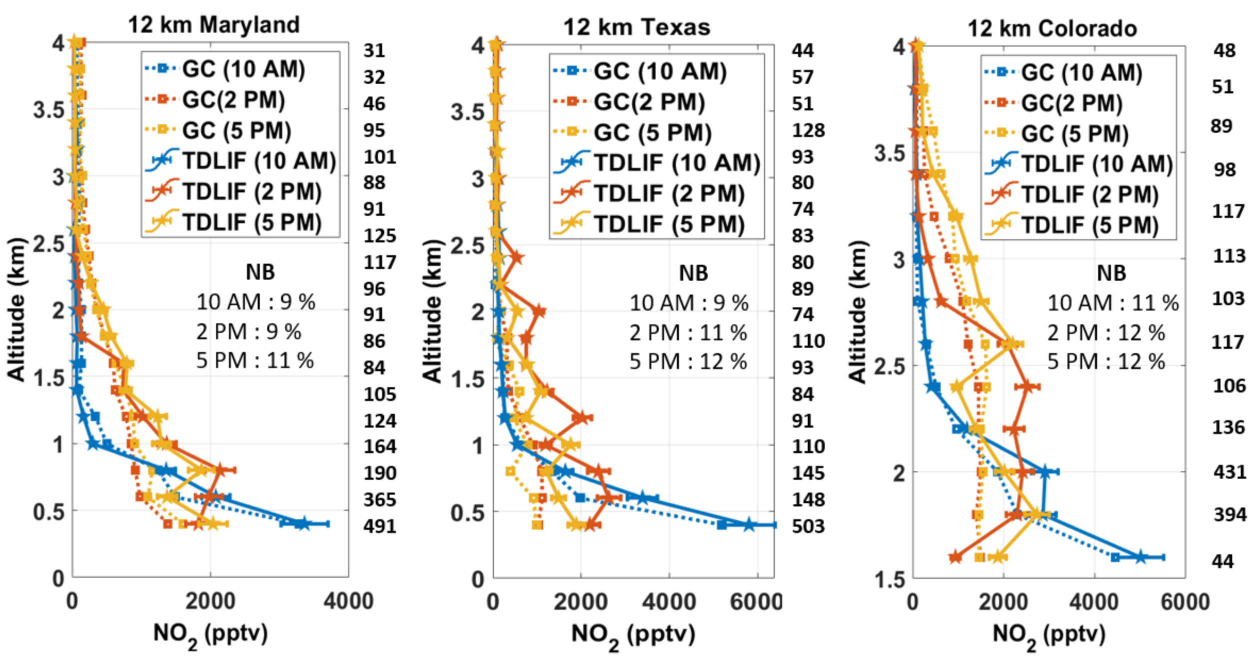

Figure A3: NO_2 Vertical profiles from TD-LIF instrument aboard during the DISCOVER-AQ campaign over Maryland, Texas and Colorado. NO_2 vertical profiles from TD-LIF instrument aboard P-3B during the DISCOVER-AQ campaign over Maryland, Texas and Colorado. The colored solid lines with pentagram markers represent observations .The dotted colored lines with square markers represent 12 km GCHP simulated mixing ratios. The inset values in the boxes show the NB at 10 AM, 2 PM, and 5 PM. The numbers in the middle represent the number the observations associated with the corresponding altitude level. Error bars indicate standard errors in measurements.

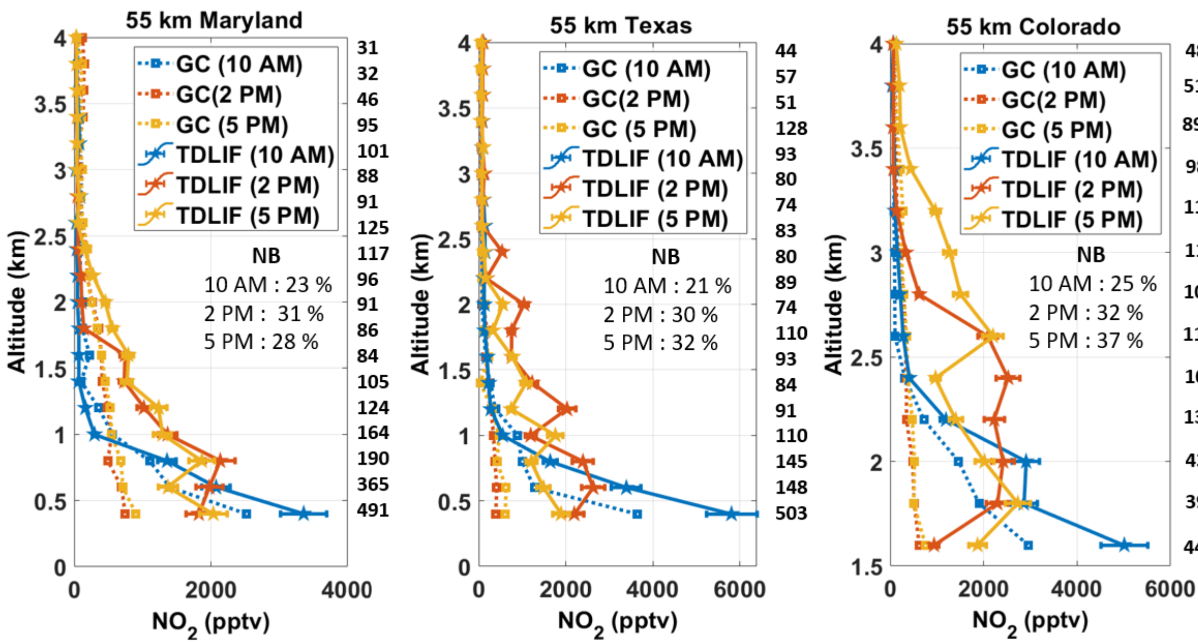

Figure A4: NO_2 Vertical profiles from TD-LIF instrument aboard during the DISCOVER-AQ campaign over Maryland, Texas and Colorado. NO_2 vertical profiles from TD-LIF instrument aboard P-3B during the DISCOVER-AQ campaign over Maryland, Texas and Colorado. The colored solid lines with pentagram markers represent observations .The dotted colored lines with square markers represent 12 km GCHP simulated mixing ratios. The inset values in the boxes show the NB at 10 AM, 2 PM, and 5 PM. The numbers in the middle represent the number the observations associated with the corresponding altitude level. Error bars indicate standard errors in measurements.

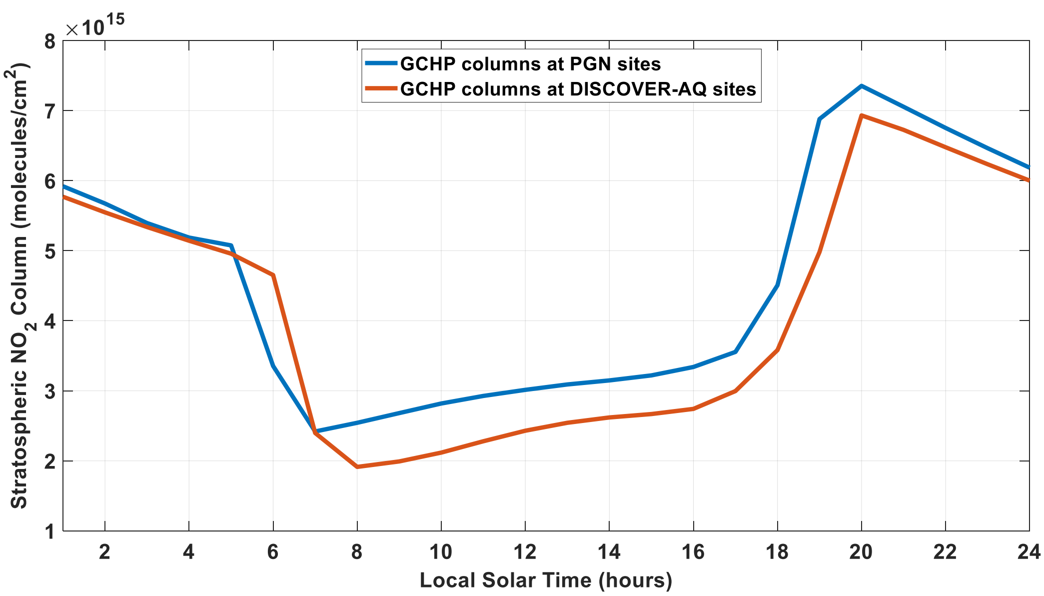

Figure A5. GCHP NO_2 stratospheric columns for the three-month average of June-July-August at DISCOVER-AQ sites (red) and PGN sites (blue).

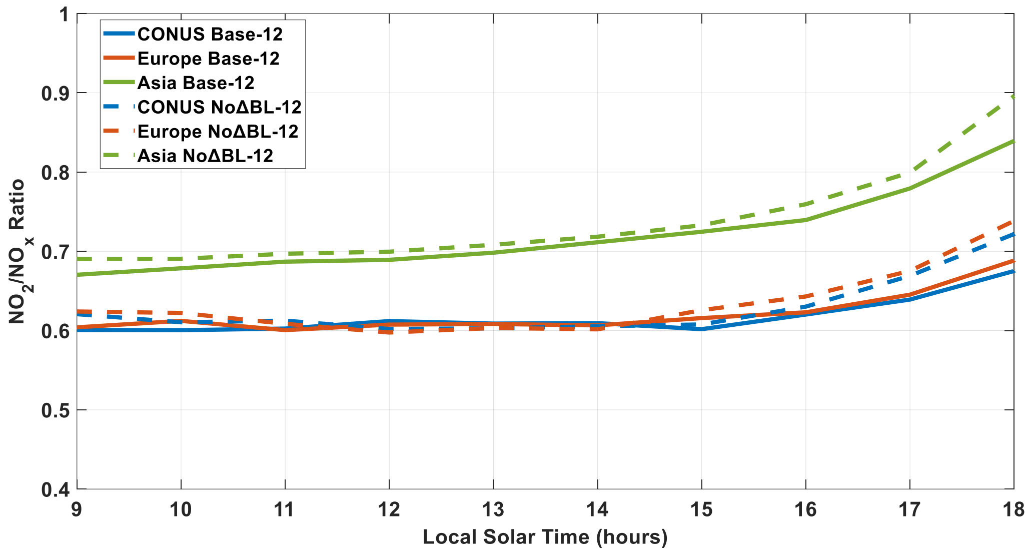

Figure A6. Hourly variation of 12 km simulated column NO_2/NOx ratios across 50 PGN sites over the CONUS (red), Europe (blue), and east Asia (green). The dotted lines show the 12 km simulated NO_2/NOx ratios without modified PBLH.

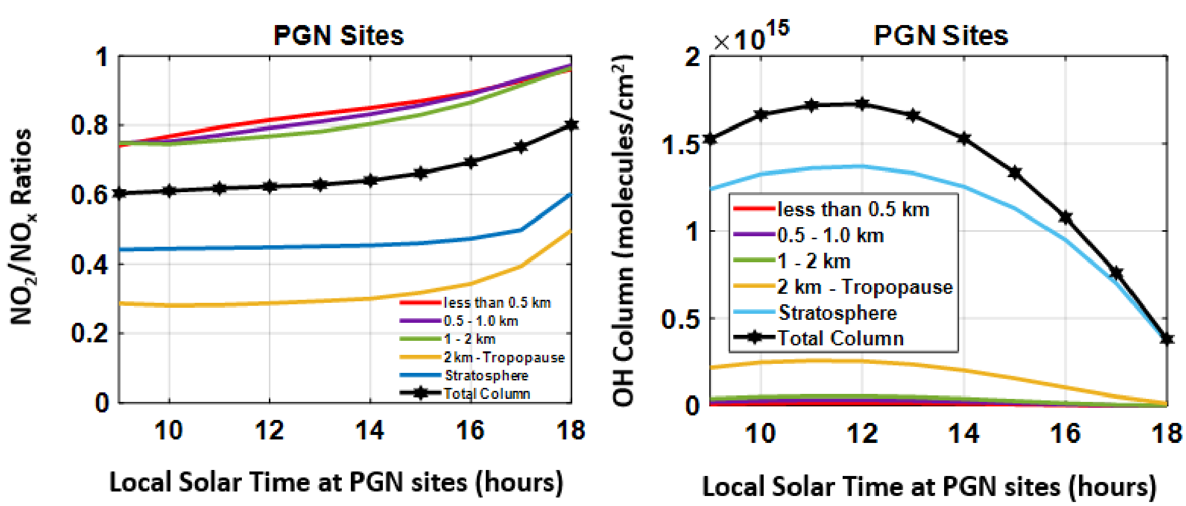

Figure A7. Simulated NO_2/NO_x ratios (left panel) and simulated partial and total OH columns (right panel) at different hours of the day averaged over the summer months of June-July-August for 2019 for PGN sites over the eastern US, western US, Europe, and eastern Asia.

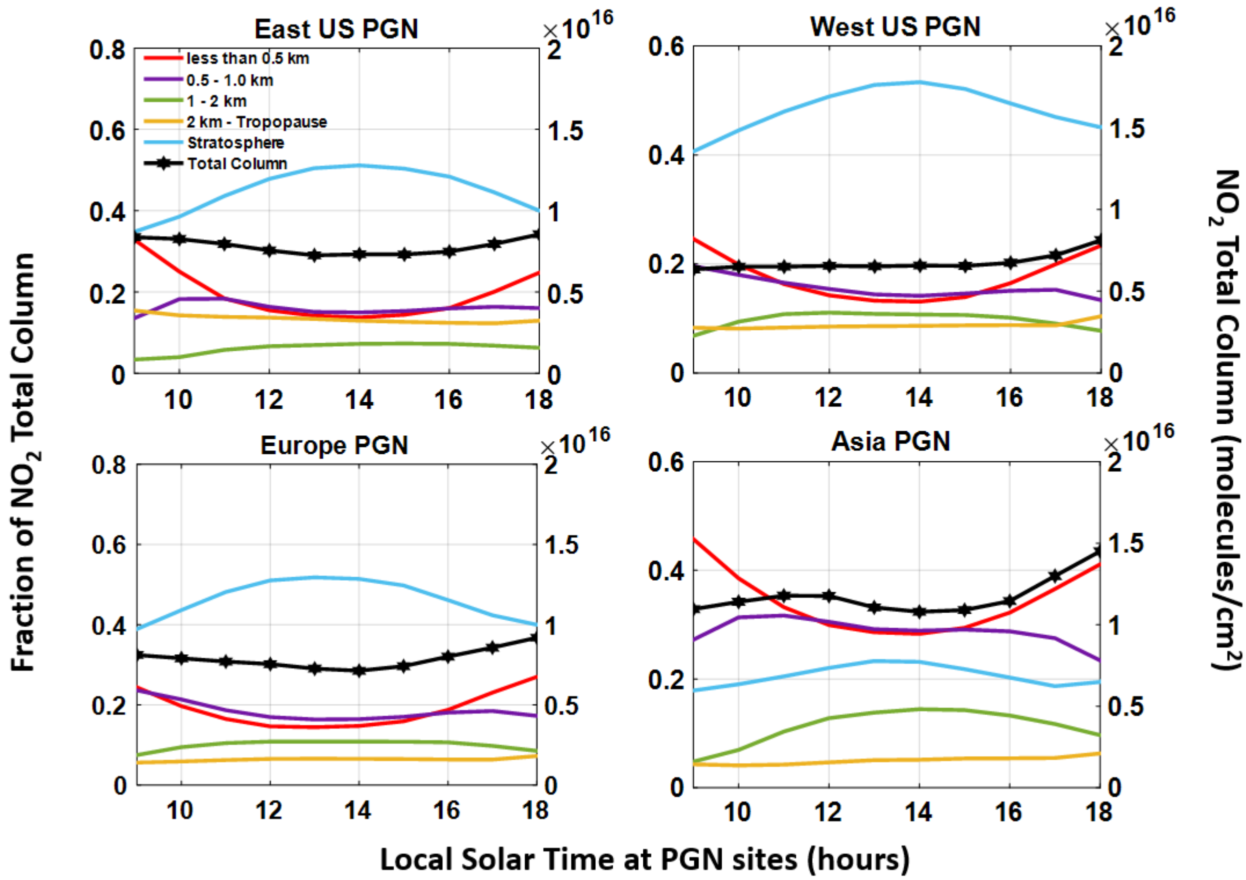

Figure A8. The simulated fractional contribution of NO_2 columns at different hours of the day averaged over the summer months of June-July-August for 2019 for PGN sites over the eastern US, western US, Europe, and eastern Asia. The right Y-axis shows the total columns of NO_2.

Table A1. Site name, latitude and longitude for 18 sites in Texas, Maryland, and Colorado that has concurrent pandora and aircraft measurements.

Site	Sites name	Latitude	Longitude	Date
	Texas Sites			September 2013
1.	Channelview	29.802	-95.125	
2.	Conroe	30.350	-95.425	
3.	Deer Park	29.670	-95.128	
4.	Galveston	29.254	-95.861	
5.	Manvel Croix	29.520	-95.392	
6.	Moody Tower	29.718	-95.341	

	Maryland Sites			July 2011
1.	Aldino	39.563	-76.204	
2.	Beltsville	39.055	-76.878	
3.	Edgewood	39.410	-76.297	
4.	Essex	39.311	-76.474	
5.	Fairhill	39.701	-75.860	
6.	Padonia	39.461	-76.631	
	Colorado Sites			July-August 2014
1.	Bao Tower	40.043	-105.012	
2.	Chatfield Park	39.535	-105.074	
3.	Denver La Casa	39.782	-105.018	
4.	Fort Collins	40.595	-105.143	
5.	Platteville	40.183	-104.734	
6.	NREL-Golden	39.743	-105.181	

Table A2. Site name, latitude and longitude for 31 sites in CONUS and 11 sites in Europe, North Africa and Middle-east, and 9 sites in east Asia from the PGN database.

Site	Site Name	Latitude	Longitude	Date
	Eastern US			June-July-August 2019
1.	'Bristol_PA'	40.1074	-74.8824	
2.	'Cambridge_MA'	42.3800	-71.1100	
3.	'CapeElizabeth_ME'	43.5610	-70.2073	
4.	'ChapelHill_NC'	35.9708	-79.0933	
5.	'CharlesCity_VA'	37.3260	-77.2057	
6.	'Dearborn_MI'	42.3067	-83.1488	

7.	'Detroit_MI.txt'	42.3026	-83.1068
8.	'Hampton_VA'	37.0203	-76.3366
9.	'Londonderry_NH'	42.8625	-71.3801
10.	'Lynn_MA'	42.4746	-70.9708
11.	'Madison_CT'	41.2568	-72.5533
12.	'Manhattan_NY'	40.8153	-73.9505
13.	'NewBrunswick_NJ'	40.4622	-74.4294
14.	'NewHaven_CT'	41.3014	-72.9029
15.	'OldField_NY'	40.9635	-73.1402
16.	'Philadelphia_PA'	39.9919	-75.0811
17.	'Pittsburgh_PA '	40.4655	-79.9608
18.	'WallopsIsland_VA '	37.8439	-75.4775
19.	'WashingtonDC'	38.9218	-77.0124
20.	'Westport_CT'	41.1183	-73.3367

Western US June-July-August 2019

21.	'Aldine_TX'	29.9011	-95.3262
22.	'Boulder_CO'	40.0375	-105.2420
23.	'Edwards_CA '	34.9600	-117.8811
24.	'Houston_TX'	29.7200	-95.3400
25.	'LaPorte_TX'	29.6721	-95.0647
26.	'Manhattan_KS'	39.1022	-96.6096
27.	'MountainView_CA'	37.4200	-122.05680
28.	'Richmond_CA'	37.9130	-122.3360

29.	'SaltLakeCity_UT'	40.7663	-111.8478	
30.	'SouthJordan_UT'	40.5480	-112.0700	
31.	'Wrightwood_CA'	34.3819	-117.6813	
	Europe			June-July-August 2019
32.	'Athens'	37.9878	23.7750	
33.	'Bremen'	53.0813	8.8126	
34.	'Brussels'	50.7980	4.3580	
35.	'Cologne'	50.9389	6.9787	
36.	'Davos'	46.8000	9.8300	
37.	'Innsbruck'	47.2643	11.3852	
38.	'Juelich'	50.9080	6.4130	
39.	'Lindenberg'	52.2900	14.1200	
40.	'Rome'	42.1057	12.6402	
41.	'Tel-Aviv'	32.1129	34.8062	
	Eastern Asia			June-July-August 2019
42.	'Beijing'	40.0048	116.3786	
43.	'Kobe'	34.7190	135.2900	
44.	'Sapporo'	43.0727	141.3459	
45.	'Seosan'	36.7769	126.4938	
46.	'Seoul'	37.5644	126.9340	
47.	'Tokyo'	35.6200	139.3834	
48.	'Tsukuba'	36.0661	140.1244	

49.	'Ulsan'	35.5745	129.1896
50.	'Yokosuka'	35.3207	139.6508

Table A3. Sectoral contribution to NOx emissions averaged over all PGN sites, the US, Europe and Asia.

PGN Sites	TRA(%)	RCO(%)	IND(%)	ENE(%)	SHP(%)	AGR(%)	WST(%)
ALL	49	19	13	7	7	4	1
CONUS	45	29	16	4	2	3	1
Europe	47	11	8	10	16	7	1
Asia	55	12	15	9	4	3	2

TRA: Transport, RCO: Residential Combustion, IND: Industry, ENE: Energy, SHP: Ship Emissions, AGR: Agriculture, WST: Waste